2000

Low bandgap α-(Si,Ge):H and α-(Ge):H devices

Zhiyang Zhou
Iowa State University

INFORMATION TO USERS

This manuscript has been reproduced from the microfilm master. UMI films the text directly from the original or copy submitted. Thus, some thesis and dissertation copies are in typewriter face, while others may be from any type of computer printer.

The quality of this reproduction is dependent upon the quality of the copy submitted. Broken or indistinct print, colored or poor quality illustrations and photographs, print bleedthrough, substandard margins, and improper alignment can adversely affect reproduction.

In the unlikely event that the author did not send UMI a complete manuscript and there are missing pages, these will be noted. Also, if unauthorized copyright material had to be removed, a note will indicate the deletion.

Oversize materials (e.g., maps, drawings, charts) are reproduced by sectioning the original, beginning at the upper left-hand corner and continuing from left to right in equal sections with small overlaps.

Photographs included in the original manuscript have been reproduced xerographically in this copy. Higher quality 6" x 9" black and white photographic prints are available for any photographs or illustrations appearing in this copy for an additional charge. Contact UMI directly to order.

Bell & Howell Information and Learning
300 North Zeeb Road, Ann Arbor, MI 48106-1346 USA
800-521-0600

UMI®

Low bandgap α-(Si,Ge):H and α-(Ge):H devices

by

Zhiyang Zhou

A dissertation submitted to the graduate faculty

in partial fulfillment of the requirements for the degree of

DOCTOR OF PHILOSOPHY

Major: Electrical Engineering (Microelectronics)

Major Professor: Vikram Dalal

Iowa State University

Ames, Iowa

2000

Graduate College

Iowa State University

This is to certify that the Doctoral dissertation of

Zhiyang Zhou

has met the dissertation requirements of Iowa State University

Signature was redacted for privacy.

Major Professor

Signature was redacted for privacy.

For the Major Program

Signature was redacted for privacy.

For the Graduate College

TABLE OF CONTENTS

ABSTRACT

In this research, α-(Si,Ge):H and α-(Ge):H devices are grown by the electron cyclotron resonance plasma-enhanced CVD technique and the electrical and optical properties of these devices under different plasma conditions are investigated.

The ion bombardment during the growth can be enhanced by low pressure, inert gas and substrate bias. The conclusion that low pressure leads to better quality of the material under hydrogen plasma because of higher ion bombardment is further verified by the space charge limited current (SCLC) method. The midgap defect density of states for the low pressure sample is lower than the one deposited under high pressure. The film properties for He-ECR films did not degrade as the pressure changed from 10 mTorr to about 25 mTorr, but at higher pressure (35mTorr). It's because the ion energy of the He plasma is higher than that of the H_2 plasma.

We also found that negative substrate bias can provide higher ion bombardment. The effects of substrate bias on the growth rate are different for the high Ge content sample and the low Ge content sample. Under certain deposition environment, the performance of the devices can be improved when a negative substrate voltage is applied. But under other conditions when the ion bombardment is already high, the effect is not so obvious.

Most researchers concentrate on the alloy with Ge content <50%. In this research, we explored the properties of α-(Si,Ge):H alloy with Ge content >50% including α-(Ge):H and found that good quality material can be obtained under appropriate plasma conditions. Fou-

rier transformed infrared absorptance spectroscopy (FTIR) measurements showed that the preference of Si-H to Ge-H is broken up, low pressure and high hydrogen dilution are beneficial to reduce Ge-Ge clustering and increase the Ge-H bond so that the material is grown more homogeneously. The quality of the α-(Ge):H material can be further improved by providing some graded boron doping in i layer and higher ion bombardment. A fill factor of 55% and Urbach energy of 40 meV are obtained for α-(Ge):H solar cell. This is the first time ever that a good quality α-(Ge):H solar cell has been made.

CHAPTER 1. INTRODUCTION

In the past 30 years, hydrogenated amorphous silicon (α-Si:H) and its alloys have attracted more and more interest due to their potential application in solar cells, photo sensors and thin film transistors [1-4]. Among amorphous silicon alloys, hydrogenated amorphous silicon germanium(α-(Si,Ge):H) has been extensively studied [5-11] because the bandgap can be easily tuned to be match to the solar spectrum. It can also be used as lower layer in multi-junction solar cells, which have higher energy conversion efficiency than single junction device. J.Yang and A.Banerjee have reported a triple junction α-Si:H and α-(Si,Ge):H solar cell with 14.6% initial and 13.0% stable (after 1000 hours light illumination) conversion efficiencies [12]. Although a lot of work has been done on the properties of α-(Si,Ge):H alloy, many aspects remained unexplored.

In Chapter 1, some basic physics of the α-(Si,Ge):H alloys will be introduced. In Chapter 2, the plasma enhanced CVD system we used to grow the materials will be described and the sample preparation and growth chemistry will be mentioned. In Chapter 3, a set of systematic diagnostic measurement techniques will be explained. In Chapter 4, the effect of the ion bombardment on the α-(Si,Ge):H devices and the properties of low bandgap α-(Si,Ge):H and α-(Ge):H device will be discussed. In Chapter 5, some important conclusions will be drawn.

1.1 Physics of α-(Si,Ge):H alloy

1.1.1 Structural properties of α-(Si,Ge):H alloys

Unlike crystalline, amorphous semiconductors do not have long range order. Many concepts such as lattice, point defect and Bloch wave are not applicable. The structural model of α-(Si,Ge):H can be described as a continuous random network as shown in Figure 1.1.

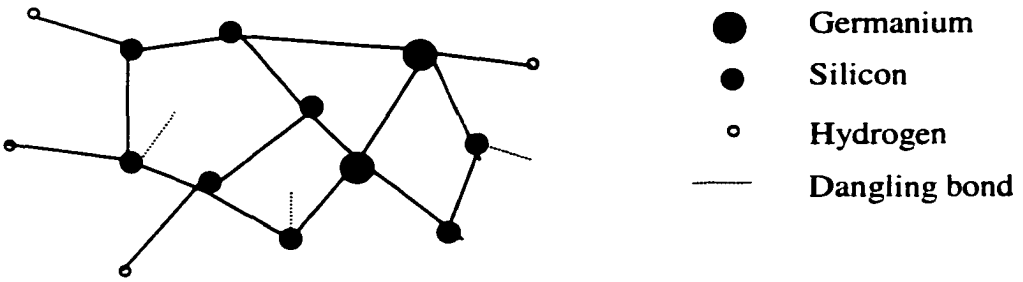

Figure 1.1 Illustration of continuous random network

In this tetrahedral network, silicon atoms bond covalently to four neighboring silicon or germanium atoms with small deviations from the bond lengths and angles of in crystalline material. The accumulation of the small deviation eventually destroys the symmetry of the structure. Some Si or Ge atoms only have a coordination number of three, leaving one unpaired electron, which is known as a dangling bond. Before passivation by hydrogen, the number of dangling bonds is about 10^{20}-$10^{22}cm^{-3}$. After passivation, the number drops down to about $7*10^{14}$ cm^{-3} for the best α-Si:H films[1]. Both dangling bonds and deviations from the bond lengths and angles will contribute to the formation of a continuous distribution of the density of states.

1.1.2 Density of states of α-(Si,Ge):H alloy

The lack of long-range order in α-(Si,Ge):H inevitably causes distortions to the tetrahedral network. It's widely believed that the bond angle and length disorder is responsible for the band tail states in the optical bandgap, while dangling bonds and small impurities are believed to cause deep midgap defect states within the optical bandgap. Figure 1.2 shows a typical electronic density of states of α-(Si,Ge):H obtained by Sutzman [5] by electron-spin resonance (ESR) in 1989.

The density of states decreases exponentially from the conduction band edge or valence band edge. The inverse of slope of the conduction band tail is about 25 meV, while the inverse of the slope of the valence band tail is about 45-55 meV.

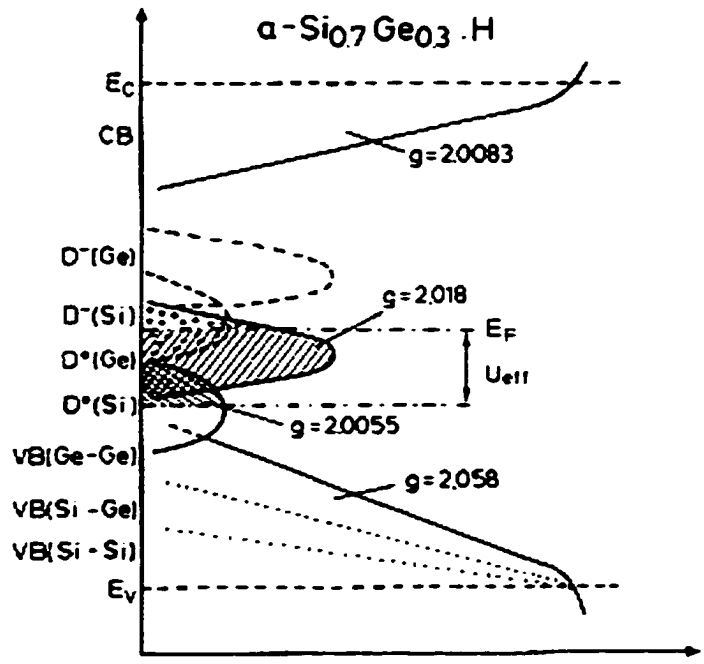

Figure 1.2 DOS in α-($Si_{0.7}Ge_{0.3}$):H (Stutzman, J.Appl.Phys., 1989)

The inverse of the slope of valence band tail is also known as the Urbach energy(E_{ur}), which indicates the quality of the material. A low Urbach energy implies less disorder.

The degradation in properties of α-(Si,Ge):H alloys with decreasing E_g is due to the increasing microstructure defects by the incorporation of Ge into the material. Mahan and Raboisson [7] suggested that there is a recombination channel other than through midgap states and they correlated this excess recombination with the presence of microstructure. So the microstructure defects are very important for the properties of the material [13-18].

According to Werner Luft and Y.Tsuo's definition[1], the structure on a scale of 10 nm down to the atomic level is generally referred to as the microstructure of the amorphous film. This concept of microstructure includes aspects such as the tetrahedral network, hydrogen bonding configurations, multivacancies(up to three missing atoms), internal surfaces associated with microvoids, density fluctuations, bonded hydrogen distribution (clustered or dispersed), and unbonded hydrogen distribution (isolated and bulk molecular hydrogen). Features such as columnar structure, void volume fraction, void size distribution, void shape, and heterostructure ("islands" with low hydrogen concentration and "tissues" with high hydrogen concentration), although of micrometer scale, are also often included in the concept of microstructure. Among these aspects of microstructure defects, the following are closely associated with quality of the α-(Si,Ge):H alloy: (1) columnar structure, (2) heterostructure, (3) clustered hydrogen, (4) polyhydride bonding. Some of these attributes are interrelated.

1.1.3 Electrical and optical properties of α-(Si,Ge):H alloy

Although α-(Si,Ge):H is currently the best low bandgap material, it has much poorer electrical and optical properties than α-Si:H. By varying the Ge content in the material, the optical bandgap (E_g) of α-(Si,Ge):H alloy can be modulated from 1.8 eV to 1.0 eV. Many researchers have found that there is a linear relationship between the Ge content and optical bandgap and the quality of the material degrades with decreasing E_g [5-10]. The photoconductivity decreases and dark-conductivity increases when E_g decreases, which causes the decrease of photosensitivity as shown in Figure 1.3. Besides, with the decrease of E_g, electron and hole mobility decreases; electron mobility and hole mobility lifetime product($\mu\tau$) decreases; the Urbach energy increases and the midgap defect density of states increases.

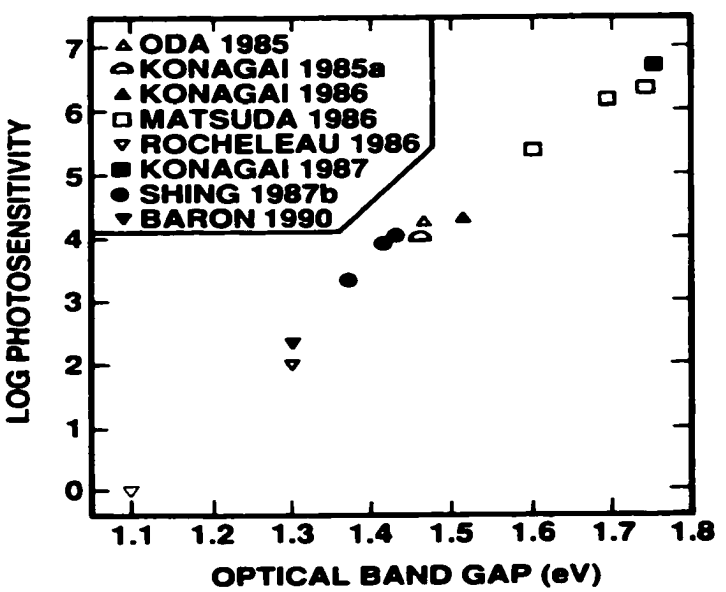

Figure 1.3 Photosensitivity σ_L/σ_D vs. bandgap[1]

Table 1.1 shows some properties of typical α-Si:H and α-(Si,Ge):H. The resulting poor photoelectric properties are generally attributed to several factors, such as preferential attachment of H to silicon rather than to germanium; increase of SiH_2 in the network; the large heterostructure present; increase of Ge dangling bonds; more Si-Si and Ge-Ge clustering; columnar structure; greater density of voids. These defects reduce transport properties.

Electrical and optical properties of α-(Si,Ge):H alloys are quite dependent on the growth methods such as RF glow discharge, photo-CVD (Chemical vapor deposition), ECR(Electron cyclotron resonance) Plasma-enhanced CVD, etc. Even when growth techniques are the same, the variation of the quality is large because of the different feed gases, different deposition conditions, different dilution etc.

Table 1.1: Some properties of typical α-Si:H and α-(Si,Ge):H

	α-Si:H.	α-(Si,Ge):H
Bandgap	1.7 eV to 1.8 eV	1.0 eV to 1.7 eV
Urbach energy	42 meV to 50 meV	≥45 meV
Photoconductivity	10^{-4} S/cm to 10^{-5} S/cm	10^{-5} S/cm-10^{-7} S/cm
Dark-conductivity	10^{-10} S/cm to 10^{-11}S/cm	10^{-9} S/cm-10^{-11} S/cm
Photosensitivity	10^{5} to 10^{6}	10^{0} to 10^{5}
μτ(hole)	$\geq 10^{-8}$ cm^2/V	10^{-8} cm^2/V to 10^{-10} cm^2/V

1.1.4 The application of α-(Si,Ge) alloys as solar cells

The main use of α-(Si,Ge) alloys is in solar cells although there are other applications such as image scanner and light emitting diodes. The structure of a solar cell is a sandwich of three layers which are phosphorus doped layer /intrinsic layer/boron doped layer. Figure 1.4 shows the band diagram of the device.

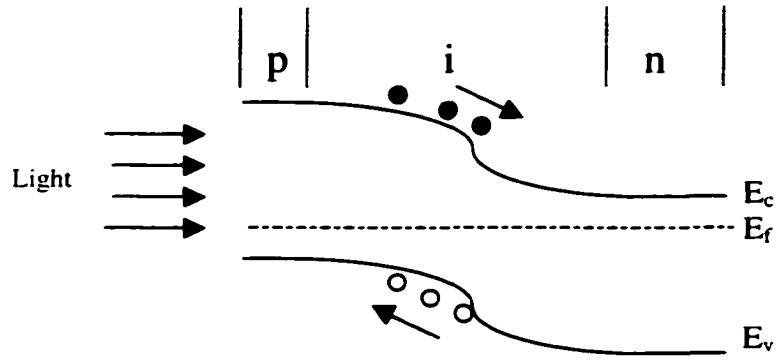

Figure 1.4 Band diagram of the α-(Si,Ge):H devices

The light is incident on the p layer and penetrates the p layer to the i layer, electrons are excited from the valence band to the conduction band by absorbing the photon energy. Because the p layer is very thin compared to the i layer, the electron-hole pairs are mainly generated in the i layer. Electrons are collected on the p side and holes are collected on the n side separately by the electric field.

The performance of a solar cell is judged by its power conversion efficiency, which is defined as the ratio of maximum power that is extracted from the cell to the total illumination power:

$$\eta = \frac{V_{\max} I_{\max}}{\phi_{in}} \text{ or } \eta = \frac{FF \cdot V_{oc} I_{sc}}{\phi_{in}}, \text{ where } FF = \frac{V_{\max} I_{\max}}{V_{oc} I_{sc}}$$

Here V_{oc} is the open circuit voltage, I_{sc} is the short circuit current. V_{max} is the voltage at the point the output power reaches maximum value, V_{max} is the current at that point. V_{oc} is mainly determined by the optical bandgap E_g, and by the quality of the material of the i-layer. I_{sc} and FF are determined by the internal electrical field and hole mobility lifetime product. These parameters will be explained in detail in Chapter 3.

The absorption of the incident light is a very critical process in a solar cell. Figure 1.5 shows the excitation of electrons from the extended states of the valence band to the conduction band, from the valence band tail to the conduction band and from the mid gap states to the conduction band.

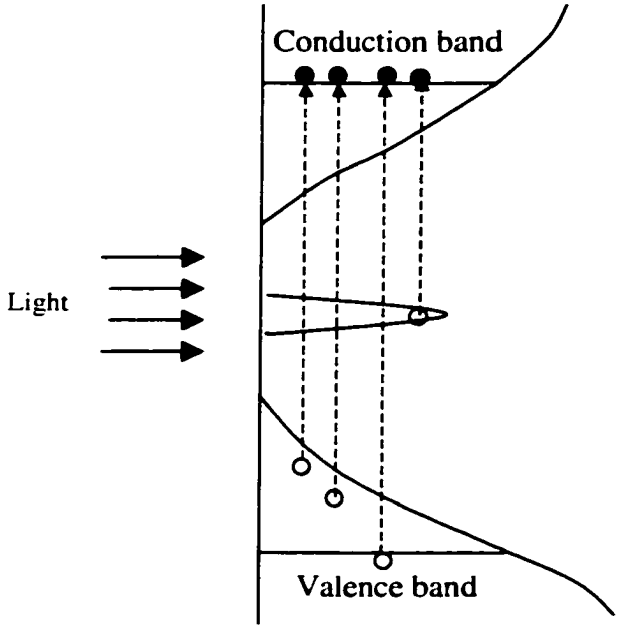

Figure 1.5 Illustration of the absorption of light

From this figure, we can find that the tail states limit the absorption of the high-energy photons and limit the open circuit voltage. The midgap states act as very effective recombination centers for excess carriers and limit the diffusion length of minority carriers and affect both fill factor and open circuit voltage. A high density of midgap defect states also reduces the electrical field in the middle of the device.

In a single junction cell, a high V_{oc} can be obtained by using high bandgap material. However, high I_{sc} can be obtained by using low bandgap material because of more absorption at longer wavelength. We can get high V_{oc} and high I_{sc} at the same time. Stacked cells can solve this problem and get high efficiency. The structure of the stacked cell is shown in Figure1.6.

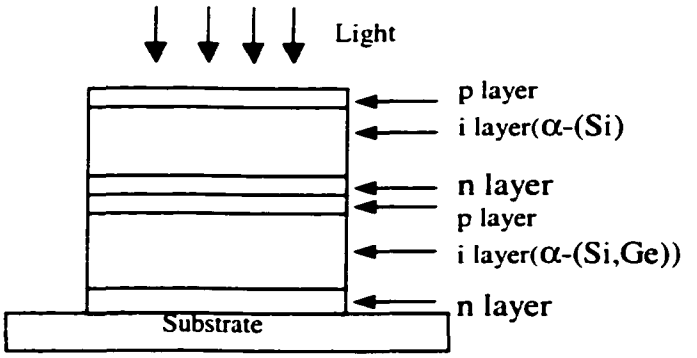

Figure1.6. the structure of the stacked solar cell

1.2 Purpose of the research

In order to improve the properties of α-(Si,Ge):H alloys, various attempts have been made to control the growth chemistry, such as use of strong dilution of H_2 and the use of fluorinated silicon and germanium reactants. It's also been suggested that good

quality α-(Si,Ge):H alloys could be deposited under conditions that maximize the ion bombardment process. Some previous work [19-27] shows that ion bombardment seems to play a role in improving the material quality.

The research group at United Solar System Corporation (USSC) showed that the electronic and optical properties of α-(Si,Ge):H films and devices deposited at high growth rate could be improved by positive ion bombardment. The ion bombardment is controlled by applying an electric bias on the substrate. In 1995, X. Xu and S.Guha[22] showed that the power conversion efficiency increased from 7.1% to 8.17% when ion bombardment was used at a high deposition rate (100Å/s). In 1996, S. Sugiyama and J.Yang [26] found that at a deposition rate between 10Å/s and 40Å/s, the fill factor of α-(Si,Ge):H solar cells has a big increase from 28% to 64% due to the high positive ion bombardment. By small angle X-ray scattering (SAXS) and infrared (IR) absorption, they found that α-(Si,Ge):H films with low ion bombardment are more porous and have higher compositions of Si-H_2 and Ge-H_2 bonding and lower total hydrogen content and that appropriate ion bombardment makes a denser structure in α-(Si,Ge):H films deposited at high growth rates. In the same year, X. Xu and J.Yang[21] reported that positive ion bombardment is not beneficial to either α-Si:H or α-(Si,Ge):H solar cells made by rf diode or triode PECVD at low growth rates. They pointed out that ion bombardment has two trade-off effects: (1) increased adatoms mobility gives rise to a denser structure and superior material quality, and (2) ion bombardment induced defects cause deterioration in carrier transport properties. The performance of the α-(Si,Ge):H

solar cell can be optimized by adjusting these two effects and in low deposition rate material, the second factor dominates, while the growth rare is high, performance is limited by poor adatom mobility and ion bombardment is desirable.

Paul Wickboldt and Dawen Pang[23] at Harvard university showed that electronic and optical properties of films are improved by ion bombardment. They found that the elimination of heterogeneous, columnar-like structure is attributed to increased ion bombardment during growth and conditions which also yield a high electron temperature in the discharge plasma, resulting in favorable discharge chemistry. They grew the sample by rf diode PECVD at 8Å/s and their research was limited to films.

The work from both groups is incomplete and sometimes contradictary. We have questions like: Under what conditions does ion bombardment have a strong effect on material and device properties? Can we further improve the material at low growth rates? And do the changes in plasma conditions imply more ion bombardment, or is something else going on?

The second goal of this research is to get good quality materials with lower bandgaps. It's generally believed that when the Ge content is larger than 50% in the alloy, the quality of the material is much worse. Most of the researchers concentrate on the α-(Si,Ge):H alloy with Ge content less than 50%. We investigated if we could use a combination of hydrogen dilution, growth chemistry and ion bombardment to produce a good low bandgap α-(Si,Ge):H and α-(Ge):H device.

CHAPTER 2. SAMPLE PREPARATION AND GROWTH CHEMISTRY

2.1 ECR PECVD system

The samples are prepared by electron cyclotron resonance (ECR) microwave remote plasma enhanced CVD technique. Compared with the conventional glow discharge technique, ECR plasma CVD has some advantages [1]:

(1) Efficient energy transfer from microwave field to the plasma

(2) Control of the ion energy typically(10-50 eV) by the gas pressure to avoid high-energy particle bombardment of the growing film, thereby producing less stress in the film and less damage to the growing surface.

(3) High utilization of the feedstock gases

(4) Better control of the dissociation of the deposition gas

(5) Lower operating pressure, which may lead to cleaner processing

(6) Lower substrate temperature

(7) Reduced powered electrode effects, such as contamination, self-biasing, and hot electron generation

(8) High ionization ratio (10^{-2})

(9) High plasma density ($>10^{11}/cm^3$)

These advantages make ECR-PECVD a good technique especially in alloy growth.

The schematic diagram of the reactor is shown in Figure 2.1. It consists of a microwave source operating at 2.45 GHz, which feeds power through a 3-stub tuner into the cavity. The plasma gases are introduced into the microwave cavity near the source end and the reaction gases are introduced into the chamber near the substrate through a separate manifold. The circular motion of the electrons is caused by the magnetic field provided by the two coils. The plasma is excited by these high-energy electrons. When the frequency of the cyclotron electrons is equal to that of the microwave source, most of the energy is absorbed by the plasma. The plasma enters the reaction chamber through the restricting orifice and then decomposes the reaction gases. Then the film is grown when these reactive radicals reaches the substrate. The substrate temperature can be controlled by an electrical heater.

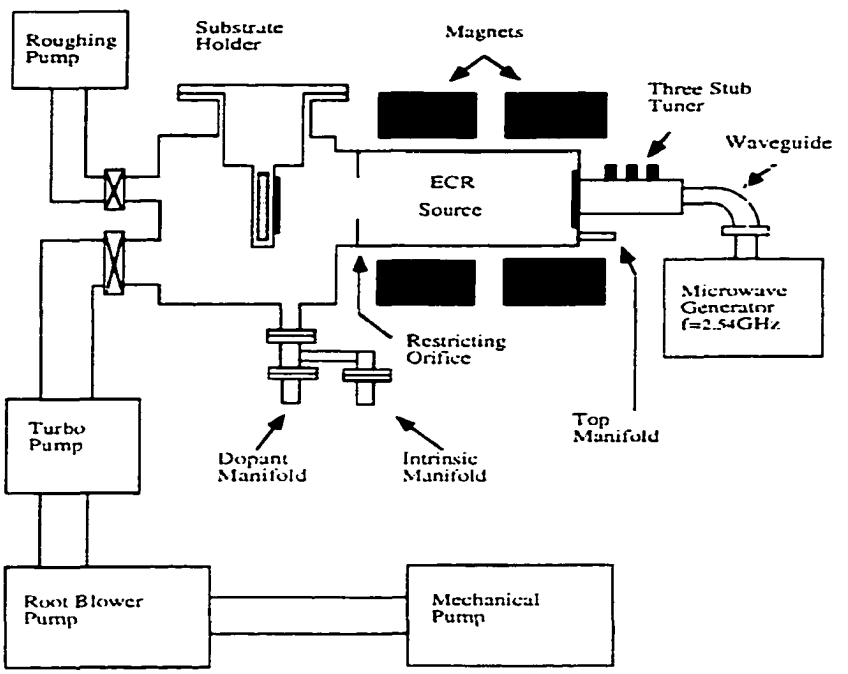

Figure 2.1 The schematic of the ECR system[28]

2.2 Sample preparation

In this experiment, 100% SiH_4 and 10% hydrogen diluted GeH_4 are used as reaction gases, H_2 or He is used as plasma gas and PH_3 or B_2H_6 as doping gas. There are three types of substrate: corning 7059 glass, stainless steel and double side polished Si wafer. Corning 7059 glass is used to grow films for some optical measurements. Stainless steel is used to make devices. The double polished Si wafer is used to grow films for FTIR measurements.

The geometry of the two different kinds of devices made in the ECR reactor is shown in Figure 2.2 and 2.3. The p-i-n device is an SS/n+/i_2/i_1/p structure and is used as a solar cell. The n-i-n device is an SS/n+/i/n structure and is used to measure the midgap defect density.

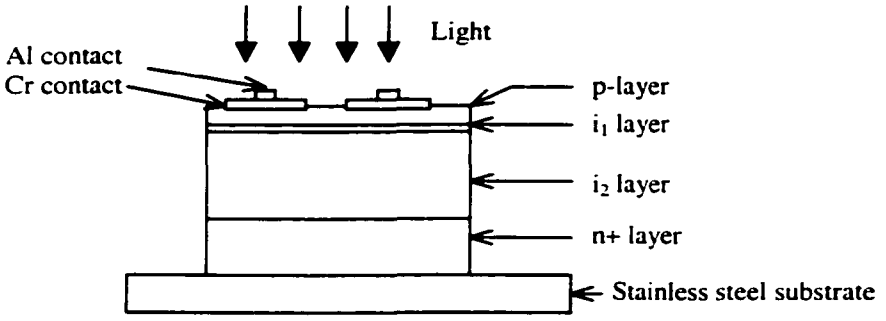

Figure 2.2 Geometry of p-i-n devices

For a p-i-n device: the thickness of the phosphorus doped n+ layer is about 0.45-0.55μm and the thickness of the intrinsic i_2 layer is from 0.15-0.5μm. I_1 is a very thin buffer layer which used to make a transition in bandgap between the p-layer and the i-layer as well as limiting the diffusion of boron from the p-layer to the intrinsic layer.

The last layer, boron doped p layer, is about 0.05μm thick and the bandgap is higher because of the addition of carbon into the p-layer. The high bandgap p-layer reduces optical losses in the p layer and also reduces back diffusion and recombination of carriers. A semi-transparent Cr and a narrow Al bar are deposited by evaporation, which are about 0.01 μm and 0.1 μm thick respectively.

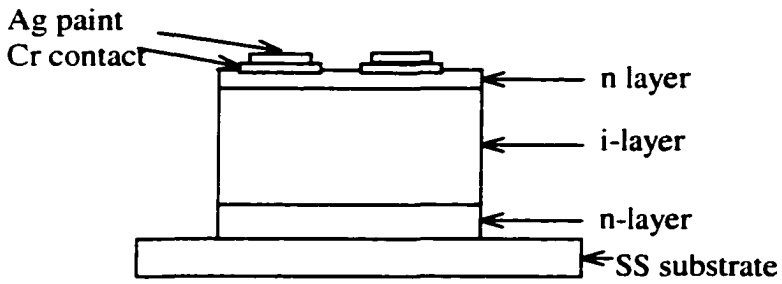

Figure 2.3 Geometry of n-i-n devices

For n-i-n devices: the differences are that there is no i_1 layer and the upper layer is n+ layer again, not p layer. The thickness of the intrinsic layer is about 1μm. Cr of 0.1μm thick is deposited by evaporation and a thin layer of silver paint are followed as contact.

2.3 Growth chemistry

The growth chemistry is very important for the quality of the material [35-41]. A good growth mechanism will result in a better material. The ion flux reaches the surface of the substrate and forms a thin layer of amorphous material. There are several reactions near the surface:

$e^- + SiH_4 \rightarrow SiH_3 + H^+$

$e^- + SiH_3 \rightarrow SiH_2 + H^+$

$e^- + SiH_2 \rightarrow SiH + H^+$

$H^+ + SiH_4 \rightarrow SiH_3 + H_2$

$e^- + GeH_4 \rightarrow GeH_3 + H^+$

$e^- + GeH_3 \rightarrow GeH_2 + H^+$

$e^- + GeH_2 \rightarrow GeH + H^+$

$H^+ + GeH_4 \rightarrow GeH_3 + H_2$ (2.1)

If all the three species (XH_3, XH_2, XH) (X=Si or Ge) are present equally, the surface will be rough and many microvoids and dangling bonds will be formed. It is preferred that only one species dominates. In the ECR PECVD system, XH_3 and XH_2 are the major radicals. If we use high hydrogen dilution, then reaction 1 and 4 are predominant and XH_3 will be the major radical. Besides, hydrogen has other effects during the growth: passivate the dangling bonds, etch the surface hydrogen, break the weaker Si-Si and Ge-Ge bonds (etching during growth) etc [35-41].

With the addition of Ge into the alloy, the defect density increases compared to the density in α-(Si):H. This result is believed to arise from the following factors: (1) Growth from many radicals, the inhomogeneous growth leads to poor microstructure (2) Ge is heavier than Si, so the surface mobility of Ge is very low. The relative growth rate of Ge is higher, so there is a preference of Ge into the alloy (3) The Si-Si bond is 2.3eV,

Ge-Ge is 1.9eV, Si-H is 3.35eV, Ge-H is 2.99eV, so there is a preference of Si-H to Ge-H, leaving more Ge dangling bonds.

The question that arises is: How to improve the quality of α-(Si,Ge):H alloys? The discussion of growth chemistry shows that three parameters may be important in producing better films: (1) High hydrogen dilution: reduce the Si and Ge dangling bonds, (2) Optimize the deposition parameters such as pressure, power and temperature (3)Ion bombardment: provide mobility to radicals on the surface by collisional momentum transfer so as to improve the microstructure of the material.

CHAPTER 3. CHARACTERIZATION

In this thesis, a set of systematic measurement methods is used to get the characteristics of both films and devices. Among them, the midgap defect density measurement is new and first used in our group, while other measurements will be described simply because they had been covered in previous theses [27][28][34].

3.1 Films

3.1.1 Thickness

The thickness of the films is measured by λ-9 dual beam spectrophotometer. Figure 3.1 shows the transmittance of a α-(Si,Ge):H film that has a Tauc gap of 1.56eV. The thickness can be calculated by the following equations:

$$Thickness = \frac{\lambda_1 \lambda_2}{mn(\lambda_2 - \lambda_1)} \quad , \tag{3.1}$$

where λ (>1000nm) is the value of peak or valley, n is the refractive index, m=2 for peak to peak or valley to valley intervals and m=4 for peak to valley or valley to peak intervals.

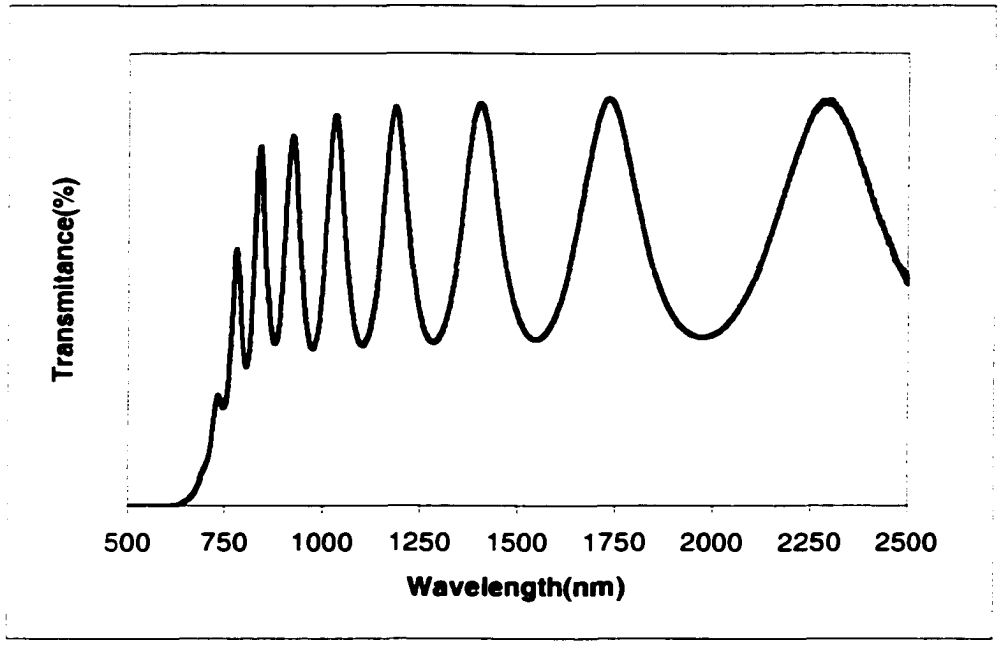

Figure 3.1 Transmittance of α-(Si,Ge):H film

3.1.2 Bandgap

There is a relationship between absorption coefficient and optical bandgap of the film. It can be described by the following equation, which is for photon energies larger than the optical bandgap:

$$\sqrt{\alpha \cdot h\nu} = B(h\nu - E_g) \ . \qquad (3.2)$$

The optical bandgap defined by this equation is called the Tauc gap. In Figure 3.2, the intersection of the dashed line with the x-axis shows the Tauc gap. The bandgap can also be determined by the photon energy at which the absorption coefficient is 10^4 cm^{-1}, which is called E_{04} (as shown in Figure 3.3) The difference between E_{tauc} and E_{04} is that the Tauc gap is thickness dependent, while E_{04} is independent of the thickness.

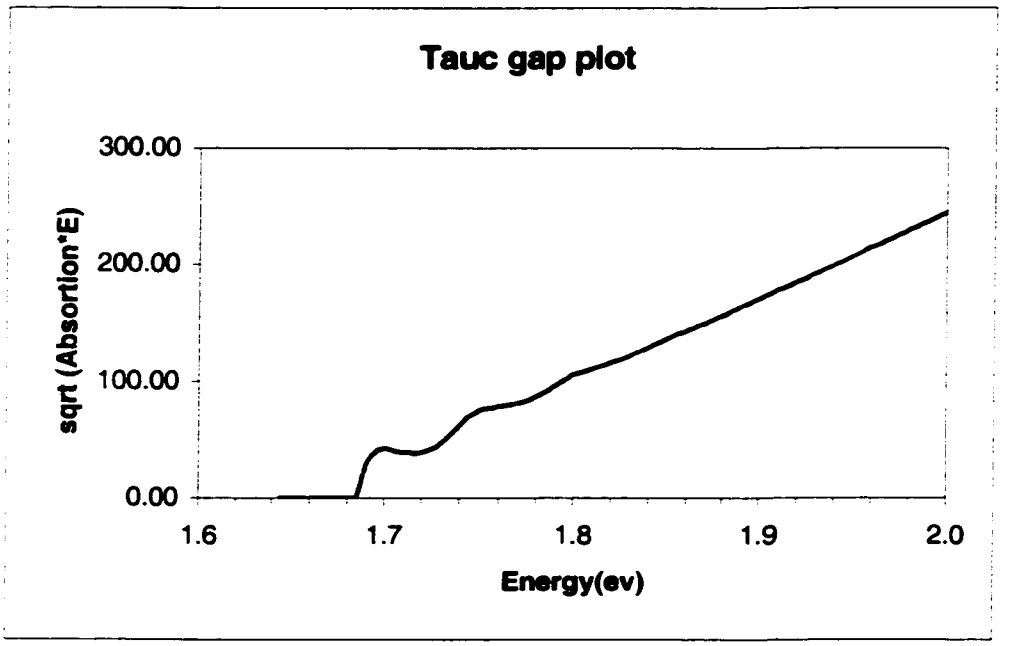

Figure 3.2 Tauc gap plot of α-(Si,Ge):H film

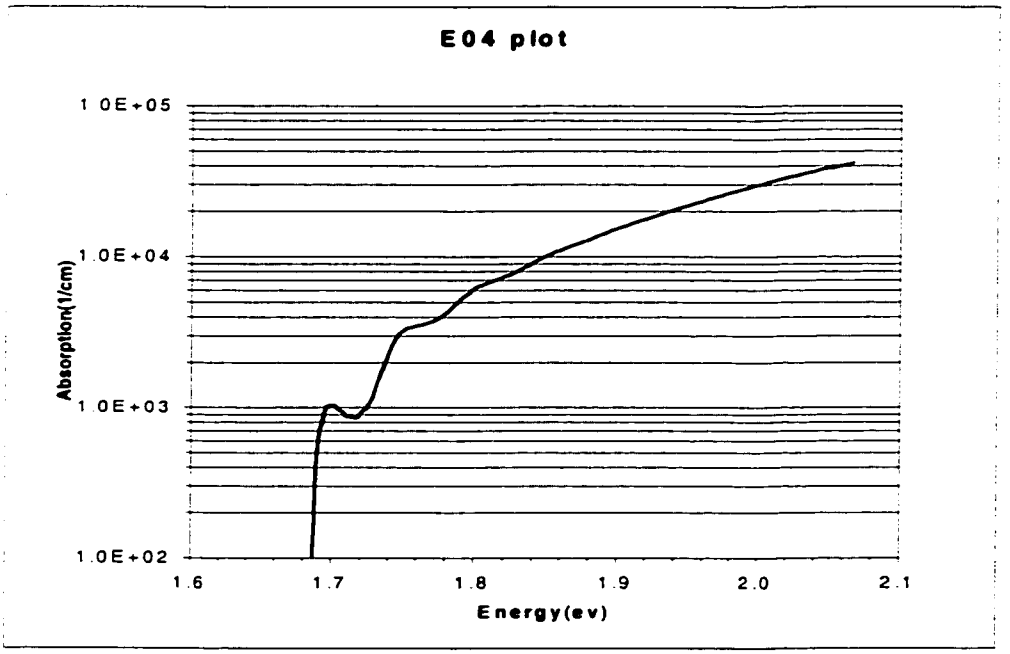

Figure 3.3 E_{04} plot of α-(Si,Ge):H film

3.1.3 Photo and dark conductivity

The ratio of the photoconductivity to dark conductivity is called photosensitivity, which is an indication of the quality of the material, along with the photoconductivity. The photo and dark conductivity are determined in our lab by the applying a voltage on the two parallel metal contacts. The conductivity can be deduced by the following equation:

$$\sigma_{l,d} = \frac{W}{L} \cdot \frac{I}{V \cdot d}, \tag{3.3}$$

where W/L is the length to width ratio of the metal contact, d is the thickness of the film, V is the applied voltage and I is the current.

3.1.4 Electron quantum efficiency, mobility and lifetime product

The photoconductivity normalized against the actual amount of light absorption is equal to the product of quantum efficiency, mobility and lifetime of electrons ($\eta\mu\tau$). The simplest form of photoconductivity can be expressed as:

$$\sigma_{Ph} = \Delta n q \mu, \tag{3.4}$$

where

$$\Delta n = G \cdot \tau = \alpha(1-R)\eta\tau\phi_{in}, \tag{3.5}$$

$$\sigma_{Ph} = \alpha(1-R)\phi_{in} q \eta\mu\tau. \tag{3.6}$$

So the electron $\eta\mu\tau$ can be obtained by the measurement of photoconductivity.

3.1.5 Sub Bandgap absorption

Unlike crystalline Si, there is still some absorption below the optical bandgap because of the existence of the band tail and the midgap defects (shown in Figure1.3). The relation between absorption coefficient and incident photon energy when photon energy is below the bandgap is defined as:

$$\alpha = \alpha_o \exp(\frac{h\nu - E_g}{E_{ur}}). \tag{3.7}$$

The inverse of the slope of the curve is the Urbach energy we mentioned before. Figure 3.4 shows the absorption coefficient vs. incident photon energy. The curve can be divided as three regions: The curve follows the first equation for α when $E>E_g$, and then the E_{ur} equation when $E_{midgap}<E<E_g$ and the absorption in the third region is because of the existence of the midgap defects.

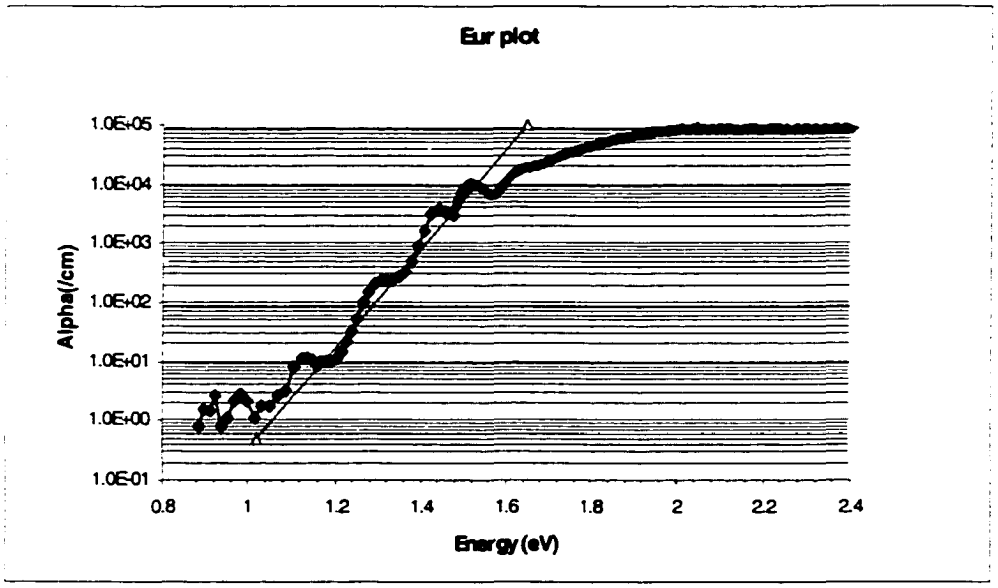

Figure 3.4 Absorption coefficient vs. Incident photon energy

3.1.6 Activation energy

The activation energy E_a is an indication of how intrinsic the material is. It can be obtained by the measurement of dark conductivity at different temperature. The relationship between dark conductivity and activation energy is expressed by:

$$\sigma = \sigma_0 \exp(-\frac{E_a}{kT}) . \qquad (3.8)$$

3.2 Devices

The performance of solar cell can be characterized by the following characteristics.

3.2.1 J-V curve(V_{oc}, J_{sc}, FF)

The equivalent circuit of the device is shown in Figure 3.5.

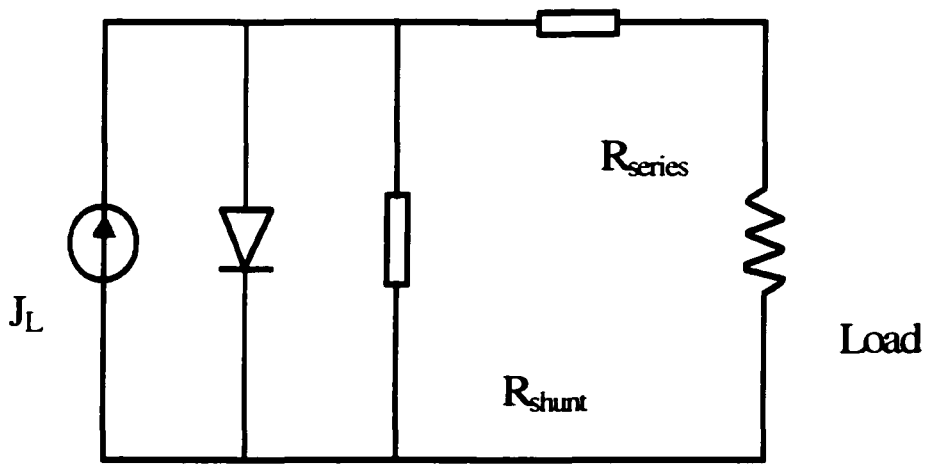

Figure 3.5 Equivalent circuit of p-i-n devices

The circuit consists of a current source, a diode and series and shunt resistances. A typical J-V curve of the α-(Si,Ge):H solar cell is shown in Figure 3.6. The J-V curve can be expressed by the following equation, assuming the series resistance is zero and the shunt resistance is infinite:

$$J = J_0\left(e^{\frac{-qV}{nkT}} - 1\right) - J_L \ . \tag{3.9}$$

J_0: Reverse saturation current density J_L: Current density under illumination

where

$$J_L = (1-R)\int q \cdot QE \cdot dN_{photon} = (1-R)\int_{\lambda 1}^{\lambda 2} q \cdot QE \cdot \frac{dN_{photon}}{d\lambda} d\lambda \ , \tag{3.10}$$

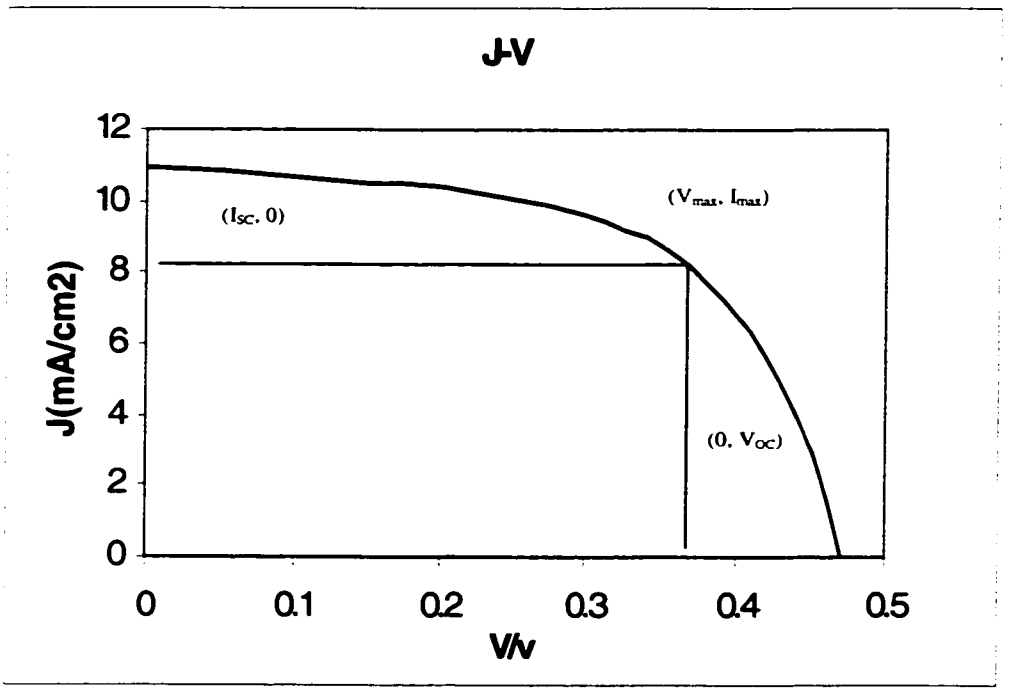

Figure 3.6 J-V curve of α-(Si,Ge):H solar cell

$$J_0 \approx \frac{q n_i^2 w_D}{\tau(n^* + p^*)} \approx \frac{q n_i w_D}{2\tau}, \tag{3.11}$$

where

$$n_i = \sqrt{N_C N_V}\exp(\frac{-Eg}{2kT}). \tag{3.12}$$

So J_L is determined by the light reflection and quantum efficiency. J_0 is determined by the bandgap and carrier lifetime.

V_{oc} is determined by the ratio of light current and reverse saturation current.

$$V_{oc} = \frac{kT}{q} Ln\left(\frac{J_L}{J_0}\right) \approx \frac{kT}{q}\left(Ln(J_L) - Ln\left(\frac{qW_d}{2\tau}\sqrt{N_c \cdot N_v}\right)\right) + \frac{E_g}{2q}, \tag{3.13}$$

so E_g is the most significant factor to change V_{oc}. If J_L or carrier lifetime τ changes by a factor of 10, V_{oc} will only changes by 60 mV. W_d is also a factor to change V_{oc}, but when the thickness of the i layer decreases, it also results in a decrease of J_L, so the effect of thickness is small and unpredictable. But a good p+/i interface and good quality material as the i layer still have positive effects on V_{oc}.

I_{sc} is determined by $I_{sc} = -J_L \cdot Area$.

FF is determined by $FF = \frac{V_{max} I_{max}}{V_{oc} I_{sc}}$, which is affected not only by the quality of the material, but also by the series resistance and shunt resistance. The effect of the series resistance can be eliminated by making a good ohmic contact. The effect of the shunt resistance is determined by the cell itself.

3.2.2 Urbach energy

Like subgap absorption, subgap QE(λ) is used to measure the Urbach energy. The curve is shown in Figure 3.7.

3.2.3 Tauc gap

The log plot of long wavelength quantum efficiency used to get the Urbach energy can also be used to estimate the Tauc gap for devices. Comparing the QE(λ) at long wavelength with an unknown E_g to another QE(λ) with a known E_g, the energy shift at the same value of QE is the difference of the two Eg if the thicknesses of the i-layer are the same. It's shown in Figure 3.7.

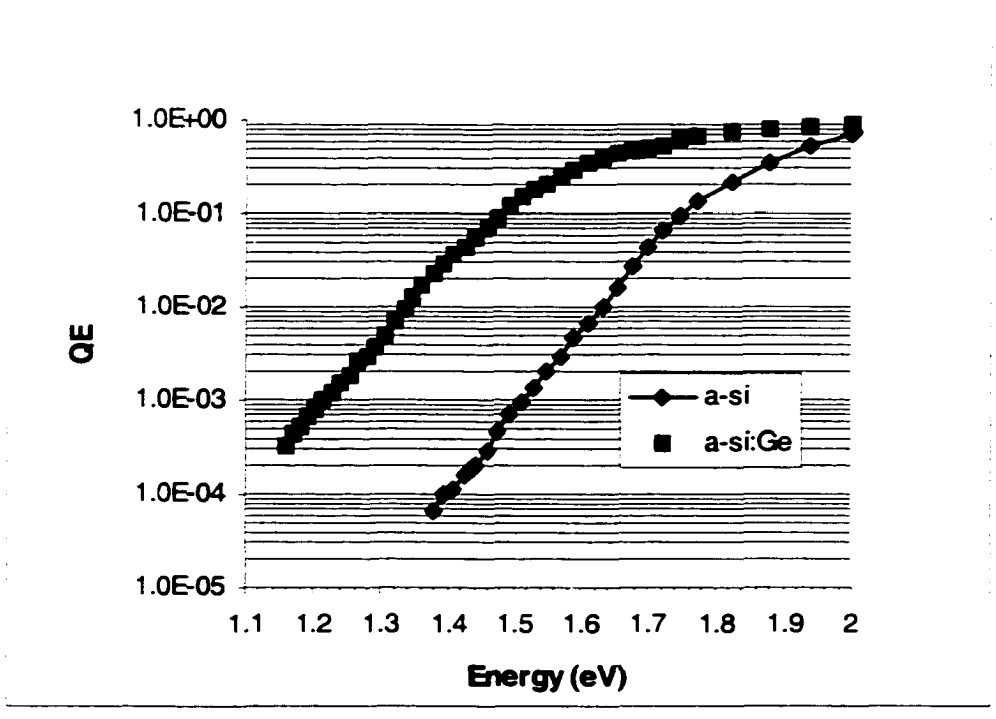

Figure 3.7 Estimation of Tauc gap

3.2.4 Quantum efficiency and Biased Quantum efficiency

Quantum efficiency is defined as the ratio of the number of charge carriers to the number of the photons incident on the sample at a certain wavelength. QE measurements provide information on how well the devices absorb photons of various wavelengths, and how well the photogenerated carriers are collected under normal forward bias conditions. The internal electric field is reduced with forward biasing, the biased QE provides details about how the reduction in E-field affects the collection of photogenerated carriers. Any problems in the device design that may inhibit carrier collection such as hole trapping at the p/i interface will be uncovered. Figure 3.8 shows an example of QE for α-(Si,Ge):H device.

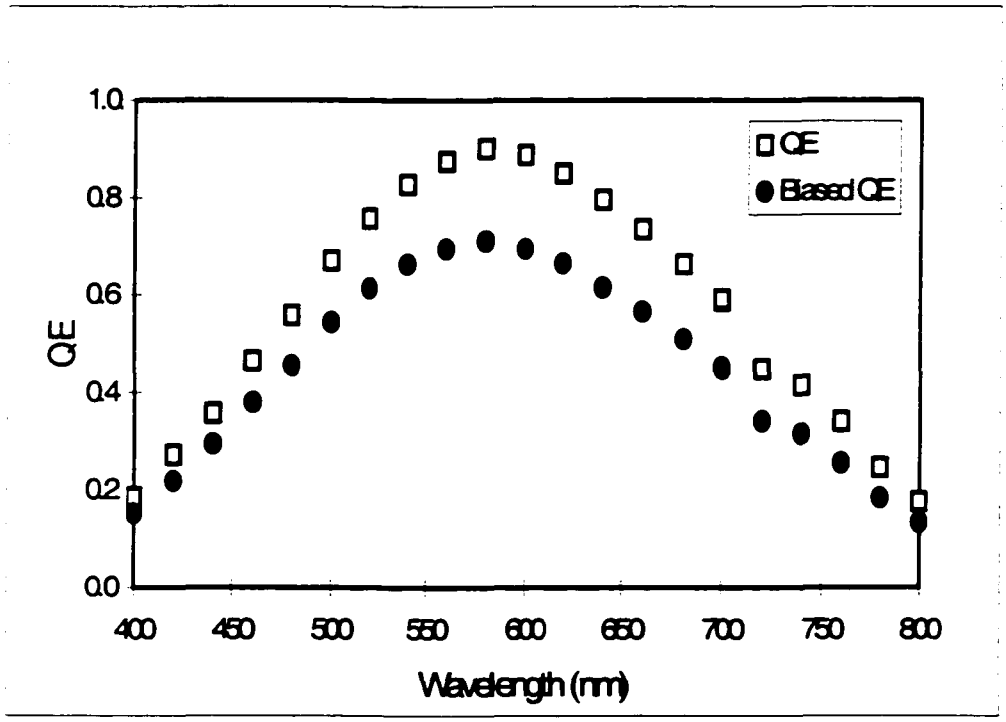

.Figure 3.8 QE and biased QE for α-(Si,Ge):H device

3.2.5 Hole mobility-lifetime product

Hole lifetime-mobility product ($\mu\tau$) shows the transportation and recombination of the holes, which is very important because solar cell is a minority devices and in most regions holes are the minority carriers [32-33]. The fill factor is primarily determined by $\mu\tau$. In order to determined the value of $\mu\tau$, we need to know the internal electric field and quantum efficiency because we have equations:

$$QE(\lambda,V)=\int_0^t \alpha(\lambda)\cdot e^{-\alpha x}\cdot e^{-\int_0^x \frac{1}{Ld(V)}dy}dx, \tag{3.14}$$

where

$$L_d=\mu\tau E(V). \tag{3.15}$$

QE can be obtained by measurement, but we can not get the electric field directly. The electric field can be solved by using Poisson's equation if the charge distribution is known. One simple method is to assume constant electric field, which is determined by $E=\frac{V}{d}$, d is the thickness of the i-layer, V is the voltage drop in the i-layer. But this assumption is not good because the actual E-field in i-layer is not constant. By using the AMPS program, the simulation results show that the E-field is high at the p-i and i-n interfaces and drops down quickly in the middle. Dalal and Haroon calculated the E-field by simply assuming that the charge density drops down exponentially from the two interfaces to the middle and the charge distribution is symmetric.

$$\frac{dE}{dx}=\frac{\rho(x)}{\varepsilon}, \tag{3.16}$$

where

$$\rho(x) = q \cdot N_0 e^{ax}, \tag{3.17}$$

$$E(x) = \frac{q \cdot N_0}{\varepsilon \cdot a} \cdot e^{ax} + E_0, \tag{3.18}$$

$$E_0 = \left(V_{built-in} - V_{applied} - \int_0^L \frac{q \cdot N_0}{\varepsilon \cdot a} \cdot e^{ax} dx \right) \cdot \frac{1}{L}. \tag{3.19}$$

The typical E-field profile from this assumption is shown in Figure 3.9.

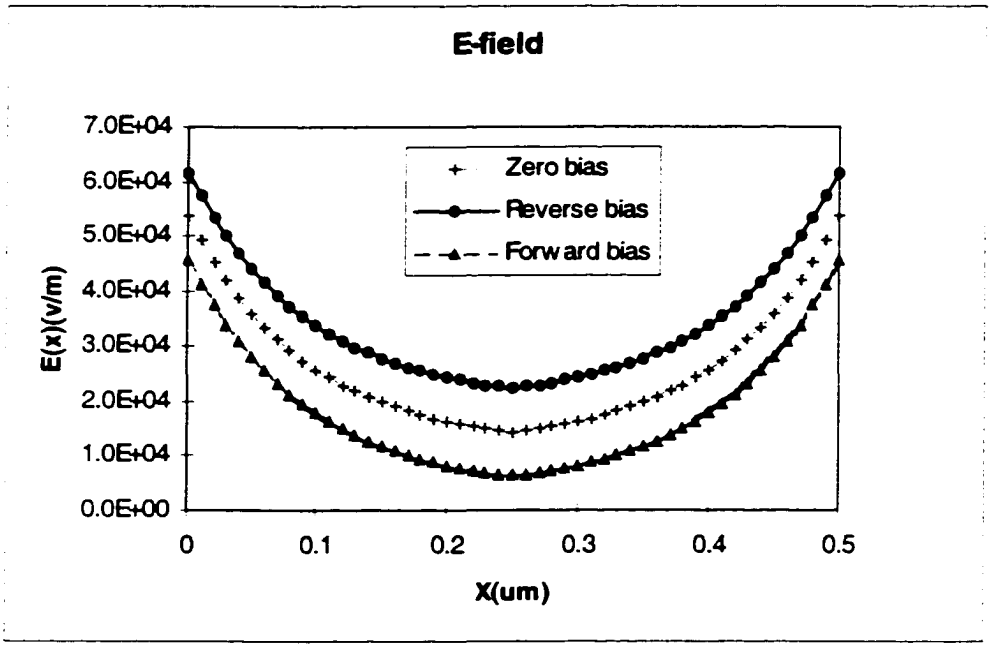

Figure 3.9 E-Filed in i-layer

Assuming that μτ does not depend on the wavelength and applied voltage, then it can be determined by fitting the QE calculation from the above equations to the QE measured. QE is measured at three different wavelength as a function of bias. Figure 3.10 shows that with μτ=7e-9, the three QE curves fit very well.

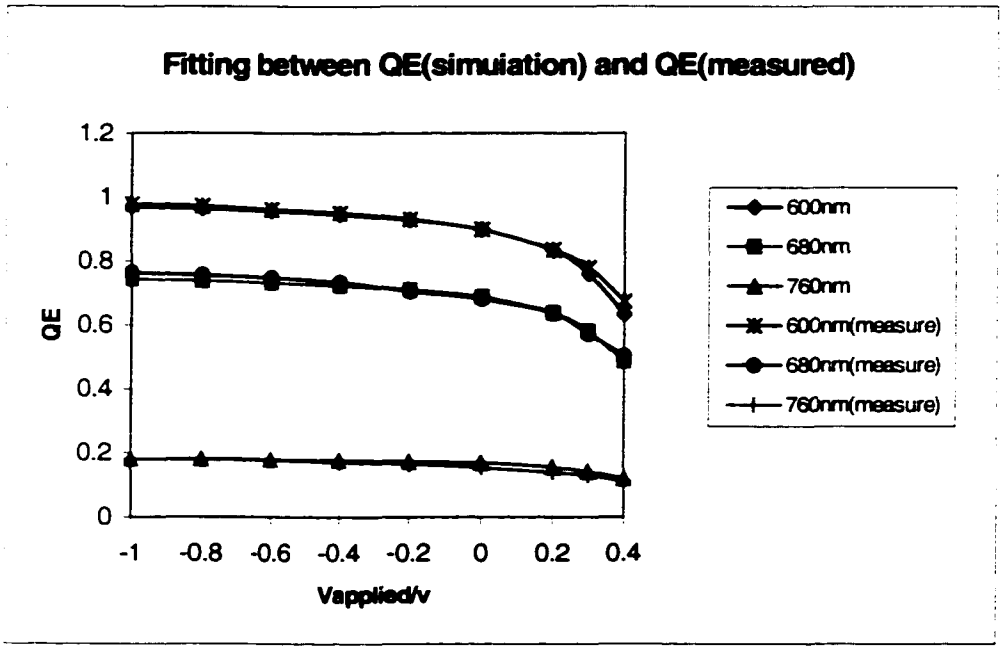

Figure 3.10 Fitting of QE curves

3.2.6 Midgap defect density

Much information on the quality and properties of a material can be obtained from its distribution of localized states, as mentioned before. There are many methods [29-31] to get the DOS such as capacitance-voltage (C-V), capacitance-temperature (C-T), field effects (FE), deep-level transient spectroscopy (DLTS) and space-charge-limited current (SCLC). The results obtained from FE are usually higher than from other methods because the FE measurement is affected by the states in the surface region. The DLTS results represent the true volume density of states, but the instrumentation and analysis is rather complex compared to other methods and several

key assumptions used to extract the DOS from DLTS spectra can't be verified and have been called into question by other workers.

Next, we will discuss the space charge limited current method. An n-i-n structure suggested by Den Boer [31] for SCLC measurements will be used. This measurement, which has not been used before in our group, gives a value for the defect density near the Fermi level and is correct within a factor of two. In the n-i-n configuration, the I-V characteristic is not obscured by exponential behavior for low voltage, as in the case of Schottky diodes. This method is thickness independent, but normally needs about 1μm for the i-layer for accuracy. A typical J-V curve measured from n-i-n devices is shown in Figure 3.11.

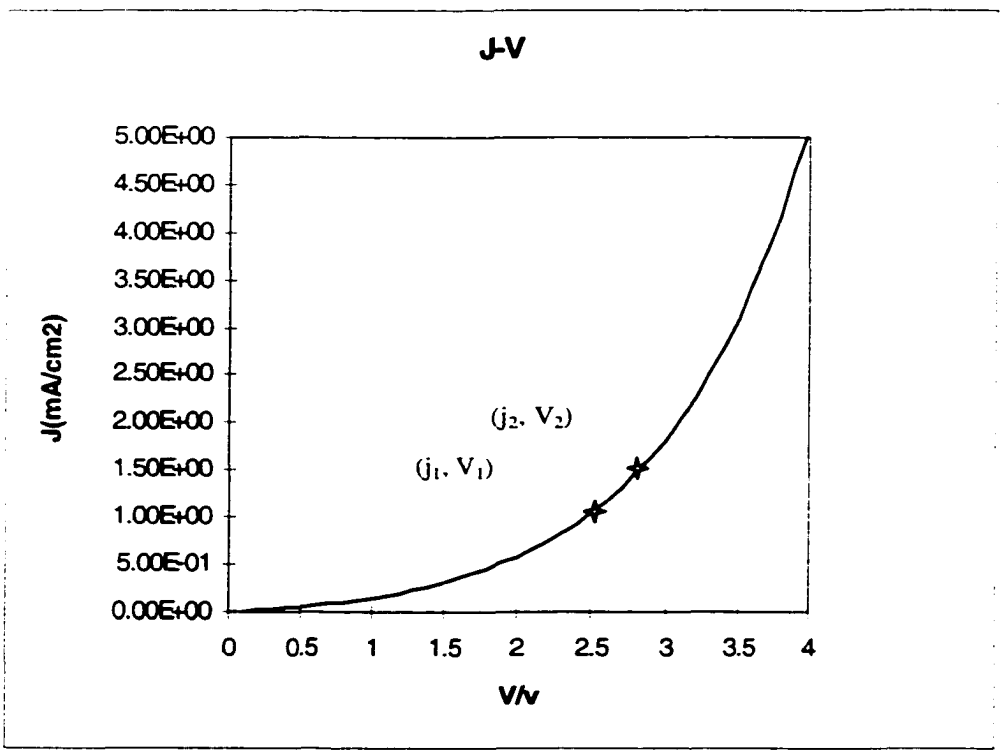

Figure 3.11 J-V curve of the n-i-n device

N (E) can be deduced from the above J-V curve using the following deductions. Assume the electric field is constant and equal to V/L, then:

$$j_1 = n_1 e\mu_n \frac{V_1}{L}, \tag{3.20}$$

where

$$n_1 = N_C \exp(-\frac{E_C - E_{F1}}{kT}), \tag{3.21}$$

$$j_2 = n_2 e\mu_n \frac{V_2}{L}, \tag{3.22}$$

where

$$n_2 = N_C \exp(-\frac{E_C - E_{F2}}{kT}), \tag{3.23}$$

where L is the thickness of i-layer. From the above equations, we can get:

$$\Delta Ef = E_{F2} - E_{F1} = kTLn(\frac{j_2 V_1}{j_1 V_2}). \tag{3.24}$$

When the electrons is injected into i layer, Fermi level rises from EF_1 to EF_2 and the number of filled trap changes. Assuming the defect density distribution $N_t(E)$ is continuous and slowly varying, the injected charge number can be expressed by:

$$N_{t2}(E) - N_{t1}(E) = \int_{E_{F1}}^{E_{F2}} N_t(E)dE \approx N_t(E) \cdot \Delta E_F , \tag{3.25}$$

Because of the assumption of constant electric field, the injected charge Q per unit area can also be expressed as:

$$Q = \frac{2\varepsilon V}{L} \quad . \tag{3.26}$$

Then we can get the defect density from the equation:

$$Q = \frac{2\varepsilon V}{L} = q \cdot L \cdot N_t(E) \cdot \Delta E_F \tag{3.27}$$

So:

$$N_t(E) = \frac{2\varepsilon_s (V_2 - V_1)}{q * L^2 * \Delta E_f} \quad , \tag{3.28}$$

the position of the defect density is determined by:

$$E_c - E_f = kT \ln(\frac{q\mu_n Nc}{j}) . \tag{3.29}$$

In this measurement, the applied electric field should be smaller than 5E4 V/m because the field ionization also contributes to the free charge density at high electric field.

3.3 FTIR measurements

Fourier transformed infrared absorptance spectroscopy (FTIR) is the measurement of the wavelength and intensity of the absorption of infrared light by a sample. Mid-infrared light (2.5 - 25 μm, 4000 - 400 cm^{-1}) is energetic enough to excite molecular vibrations to higher energy levels. The wavelength of an IR absorption band is characteristic of specific types of chemical bonds, so it's a very useful method to analyze the bonding status of silicon-hydrogen or germanium-hydrogen in our samples. The relevant peaks and their positions are shown in Table 3.1.

Table 3.1. The characteristic peaks of Si and Ge hydrogen bond

Si hydrogen bond	Wave number (cm^{-1})	Ge hydrogen bond	Wave number (cm^{-1})
Si-H stretching	2000	Ge-H stretching	1880
Si-H bending	630	Ge-H bending	570
$Si-H_2$ stretching	2080-2090	$Ge-H_2$ stretching	1980
$Si-H_2$ bending scissors	880	$Ge-H_2$ bending scissors	830
$Si-H_2$ rocking	630	$Ge-H_2$ rocking	570

CHAPTER 4. RESULTS AND DISCUSSION

4.1 Electro-optical characteristics of α-(Si,Ge):H made by ECR PECVD

It was mentioned in Chapter 1 that there is an inverse linear relationship between the Ge content and optical bandgap of the α-(Si,Ge) material. It is not easy to get the Ge content in each sample because of the complexity of the measurement. But we can measure the optical bandgap easily by measuring the optical absorption. So we can use the optical bandgap to estimate the Ge content in the material. The only deviation from this linear relationship is because of the hydrogen concentration.

When the GeH4/(GeH4+SiH4) gas flow ratio increases from 0% to 100%, that means that the Ge content goes from 0% to 100%, we got E_{tauc} decreases from 1.7eV to 1.1eV. In Table 4.1, the deposition parameters for some samples with different GeH4/(GeH4+SiH4) ratio are shown. The results are shown in Table 4.2.

Table 4.1: Deposition parameters for α-(Si,Ge):H devices

	Temperature	Pressure	Power	H2(%)	SiH4(%)	GeH4(%)	TMB(%)
2//3435	360°C	5 mTorr	100 W	60	15	30	15
2//3437	360°C	5 mTorr	100 W	60	15	40	15
2//3436	360°C	5 mTorr	100 W	60	15	45	15
2//3438	360°C	5 mTorr	100 W	60	15	50	15
2//3454	360°C	10 mTorr	130 W	60	15	20	15
2//3455	360°C	10 mTorr	130 W	60	15	30	15
2//3457	360°C	10 mTorr	130 W	60	15	40	15
2//3928	300°C	5 mTorr	150 W	60	15	40	10
2//3929	300°C	5 mTorr	150 W	60	15	60	10
2//3936	300°C	5 mTorr	150 W	60	15	80	10

With the addition of Ge into the material, the characteristics of the alloy change. We found that bandgap is the most significant factor to change V_{oc} according to the equation $V_{oc} \approx \frac{kT}{q}\left(\ln(J_L) - \ln\left(\frac{qW_d}{2\tau}\sqrt{N_c \cdot N_v}\right)\right) + \frac{E_g}{2q}$. Figure 4.1 shows the relationship between E_{tauc} and V_{oc} for all the samples (including some samples that are not shown in Table 4.1), the trendline shows that $V_{oc} \equiv A + 0.66E_g$, which is close to the estimation of the equation.

The deviation of Voc from the line results from other factors such as thickness, hydrogen content, deposition parameters etc. When the sample is very thin, the Voc is higher.

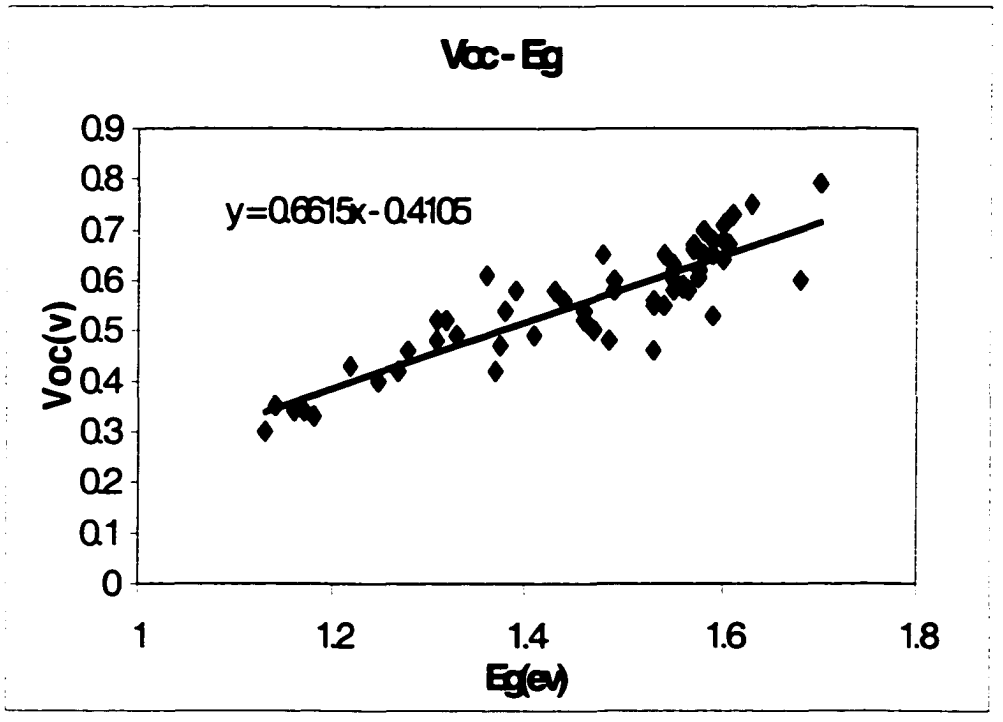

Figure 4.1 Open circuit voltage vs. bandgap

Table 4.2: Results for α-(Si,Ge):H devices

	V_{oc}(V)	I_{sc}(mA)	FF	E_{ur}(meV)	E_{tauc}(eV)
2//3435	0.68	0.305	52.30%	47.6	1.61
2//3437	0.66	0.32	52.50%	48.4	1.59
2//3436	0.63	0.52	47.80%	48.8	1.59
2//3438	0.65	0.69	46.60%	47.6	1.56
2//3454	0.79	0.55	56.60%	47.4	1.65
2//3455	0.71	0.47	59.80%	48.6	1.62
2//3457	0.66	0.355	49.80%	49.6	1.58
2//3928	0.71	0.57	57.40%	45.5	1.60
2//3929	0.60	0.71	58.60%	46.0	1.55
2//3936	0.52	0.76	54.00%	44.6	1.46

From Table 4.2, we see that Isc increases when E_{tauc} is decreasing. It's because $\alpha=B*(h\nu-Eg)^2/h\nu$, so the absorption of materials increase a lot because of the lower bandgap, that makes QE increase too and then J_L increases.

The fill factor decreases with decreasing E_g. The bond energy of Ge-H is 2.99 eV, Si-H is 3.35 eV. So it is easier to break the Ge-H bond that the Si-H bond. And because the mass the Ge atom is larger than those of Si atoms, so the mobility of gas phase GeH_x is smaller than that of SiH_x. Both these two reasons will contribute to an increasing growth rate when the GeH_4 content increases. So with less reaction time and more Ge included, the material is grown inhomogeneously. There are more defects, so the FF decreases.

Although V_{oc} and FF decreases, the power conversion efficiency is still improved because of higher Isc. This breaks the limit that α-(Si,Ge):H devices can only be applied as the bottom cell in a tandem solar cell.

E_{ur} increases, which is consistent with FF. The hole mobility lifetime product decreases, which is consistent with FF.

Figure4.2 is QE curves with different bandgaps. When the Ge content increases, quantum efficiency QE at long wavelength increases and the peak of QE move to longer wavelength. It's consistent with the decrease of E_g. When E_g is small, the longer wavelengths of the solar spectrum are used.

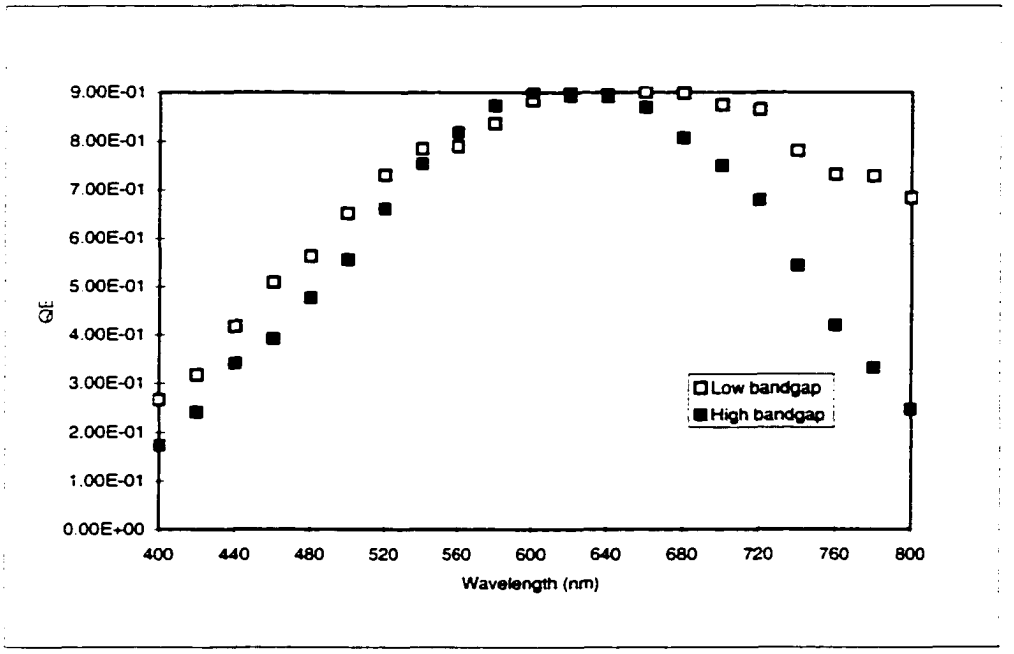

Figure 4.2 Two QE curves with different bandgap

4.2 The effect of ion bombardment on α-(Si,Ge):H devices

Ion bombardment includes both the ion flux density and the bombardment energy of the incident ions. Ion bombardment may (1) provide mobility to radicals on the surface by collision momentum transfer. (2) break up polymeric chains and increases the percentage of monohydride bonds. So ion bombardment plays an important role in the growth of the material.

The ion bombardment can be controlled by (1) deposition parameters such as pressure, power etc. (2) inert gas dilution such as He, Ar, Xe etc (3) substrate bias. In this report, the effects of pressure, He dilution and substrate bias will be discussed in detail.

4.2.1 Pressure

It has been shown in Haroon's thesis [27] that low pressure will lead to better quality of the material because of higher ion bombardment. S. Haroon and V. Dalal [36-38] showed that the α-(Si,Ge):H films and devices grown at low pressure under hydrogen plasma had better quality. Optical and electronic properties , including bandgap, Urbach energy and moblity-lifetime for both electrons and holes were found to be greatly improved at low pressure. They belieVed that the increase in ion bombardment was responsible for these effects.

In this report, the conclusion is further verified by SCLC data. Figure 4.3 and Figure 4.4 show the density of states of the films deposited at 10 mTorr and 5m Torr respectively for identical SiH4/GeH4 ratio, power and temperature.

From the two figures, the resulting density of states for samples at 10 mTorr is about $10^{17}cm^{-3}eV^{-1}$, while the density of states for samples at 5 mTorr is about $2*10^{16}$ $cm^{-3}eV^{-1}$. We can see that the defect density of states of the samples deposited under low pressure is much smaller than the one under high pressure, so the defect density of states can be reduced by the higher ion bombardment.

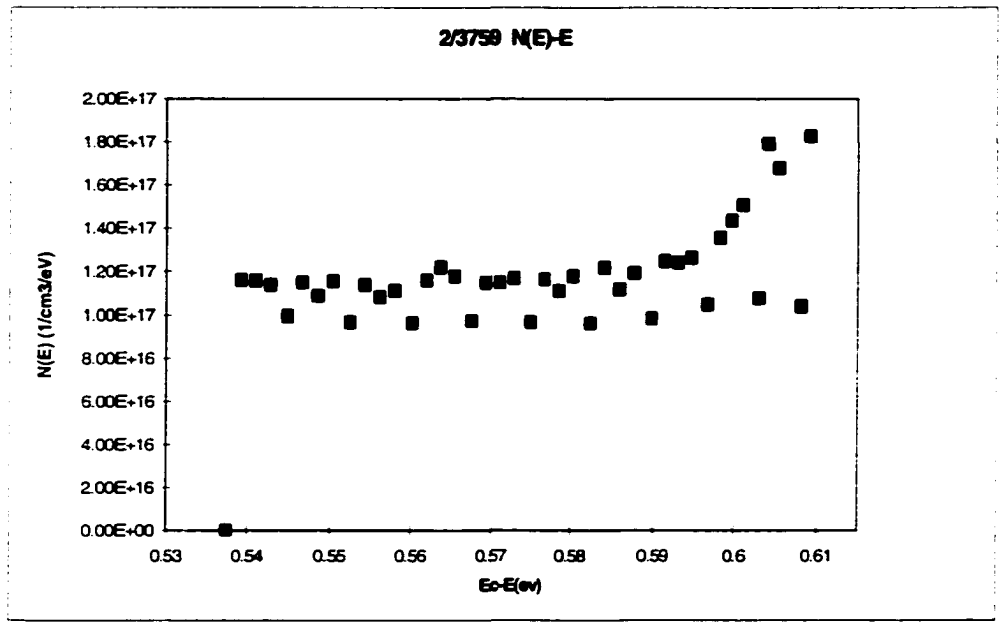

Figure 4.3 N(E) for samples at higher pressure

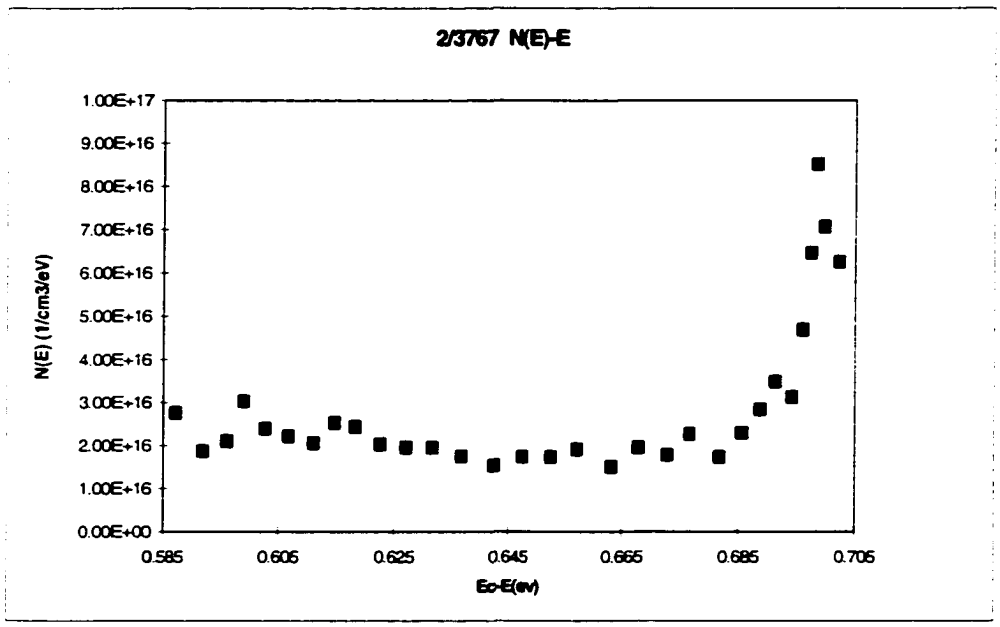

Figure 4.4 N(E) for samples at lower pressure

The density of states data found by other researchers are also presented here as a comparison with ours. Den Boers found that the midgap defect density of states for α-Si:H is about $1*10^{16}$ $cm^{-3}eV^{-1}$- $4*10^{16}$ $cm^{-3}eV^{-1}$, S.Hegedus and E. Fagen found a density of state of $1.3*10^{17}$ $cm^{-3}eV^{-1}$ and $3.6*10^{17}$ $cm^{-3}eV^{-1}$ for α-(Si,Ge):H films at Eg=1.53eV and Eg=1.3eV respectively, which are both in the order of 10^{17} $cm^{-3}eV^{-1}$. This value is much higher than the one we got at low pressure, which shows that the ion bombardment did improve the quality of the material.

4.2.2 He plasma

Some films are deposited under helium dilution. The deposition parameters are the exactly the same except the pressure (as shown in Table 4.3). The results are shown in Table 4.4.

Table 4.3: Deposition parameters for α-(Si,Ge):H films

	Temperature	Pressure	Power	He(%)	SiH4(%)	GeH4(%)
2//3167	375°C	15 mTorr	123 W	100	20	40
2//3264	375°C	25 mTorr	123 W	100	20	40
2//3166	375°C	35 mTorr	123 W	100	20	40

Table 4.4: Results for low bandgap α-(Si,Ge):H and α-(Ge):H films

	Growth Rate	E_{tauc}(eV)	E_{04}(eV)	E_{ur}(meV)	σ_L(s/cm)	σ_D(s/cm)	σ_L/σ_D
2//3167	2.26Å/s	1.58	1.75	48	1.09e-5	6.17e-10	1.77e04
2//3264	1.97Å/s	1.5	1.655	49	1.15e-5	2.49e-9	4.62e03
2//3166	1.40Å/s	1.35	1.56	62	2.44e-7	1.65e-9	1.48e02

From the results, we find that unlike the case for hydrogen plasma, the film properties for He-ECR films did not degrade as the pressure changed from 10mTorr to about 25 mTorr. However, the film properties degrade at higher pressure (35mTorr).

The reason is that the ion energy of a He plasma is higher than that of a H plasma, which is also shown in Figure 4.5. He is much more energetic than H and He is heavier than H. The momentum transfer is more effective, so the effect of pressure on ion bombardment is weak except at the highest pressures.

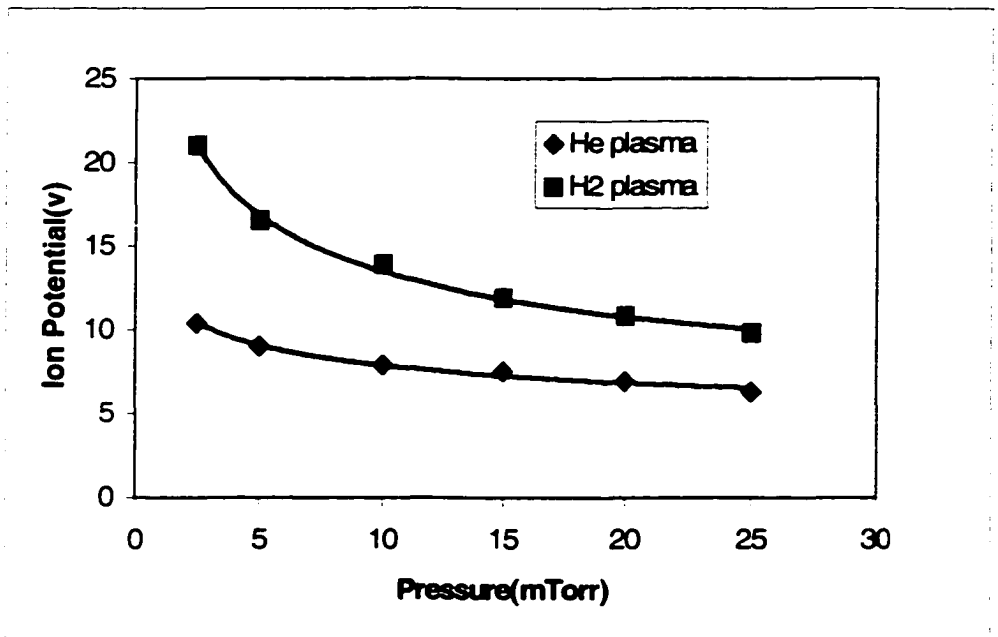

Figure 4.5 Ion potential vs. Pressure

From the samples grown under a He plasma, another interesting thing is that the bandgap of the α-(Si,Ge):H alloy increases as pressure decreases, which is unlike the situation of α-(Si):H. When there is germane existing in the environment, the strong momentum transfer caused by the He plasma increases the mobility of the radicals,

especially the heavier germyl. So the relative growth rate of Si to Ge changes, the concentration of Ge decreases and then the bandgap increases. This also shows that He does play a role in enhancing the ion bombardment by momentum transfer.

4.2.3 Substrate bias

4.2.3.1 Growth rate

At first, we need to investigate the growth rate because devices with different thickness can not be compared. So we need to know it and then control the time of deposition to get the same thickness. The growth rates under different substrate biasing have been explored at different temperature and different SiH4/GeH4 gas flow ratio. The deposition parameters are shown in Table 4.5. These samples are deposited under different Ge content, different hydrogen dilution and different temperature. The results are shown in Figure 4.6-4.8.

The growth rate is affected by two factors: the incident flux of active radicals and the surface mobility of radicals. The higher incident flux of radicals and the smaller mobility of the radicals will lead to higher growth rate.

Table 4.5: Deposition parameters for α-(Si,Ge):H films

	Temperature	Pressure	Power	H2(%)	SiH4(%)	GeH4(%)
Group 1	300°C	15 mTorr	123 W	100	15	40
Group 2	200°C	15 mTorr	123 W	100	15	40
Group 3	300°C	15 mTorr	123 W	60	15	40
Group 4	300°C	15 mTorr	123 W	100	15	80
Group 5	200°C	15 mTorr	123 W	100	15	80

The negative substrate voltage increases the ion potential, so it is easier to break the Si-H and Ge-H bonds. So the (1) incident ion flux increases, but at the same time (2) the mobility of radicals is also increasing because of high ion bombardment. For low Ge content, the first reason is predominant because the Si-H bond energy is higher and Si is not so heavy, so the growth rate increases with negative voltage (Figure 4.6 and 4.7).

But for the high Ge content, because Ge-H bond energy is smaller compared to Si-H, so the first reason is not predominant now. And because Ge is much heavier than Si, so the second reason also contributes. The result of the compensation of the two reasons is that the growth rate remains nearly unchanged with increasing negative voltage (Figure 4.8).

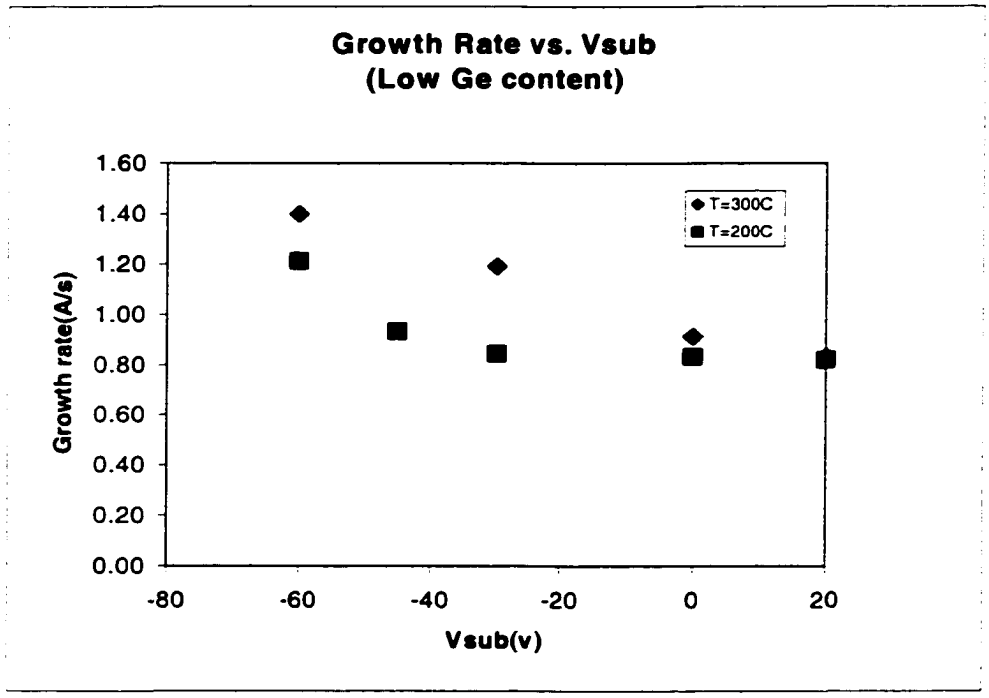

Figure 4.6 Growth rate vs. Substrate biasing for low Ge content films

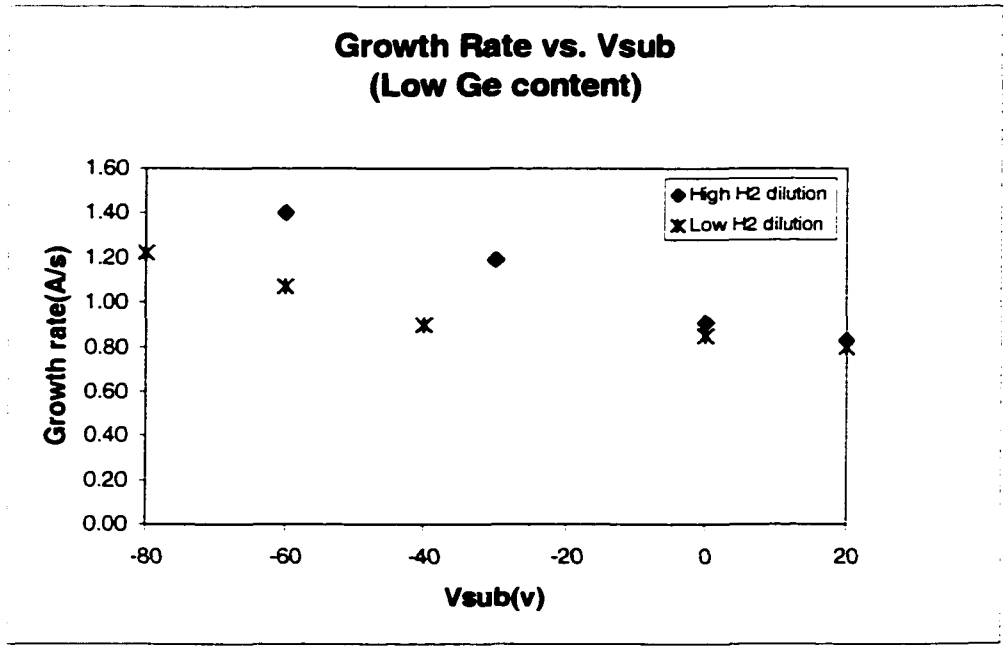

Figure 4.7 Growth rate vs. Substrate biasing for different hydrogen dilution

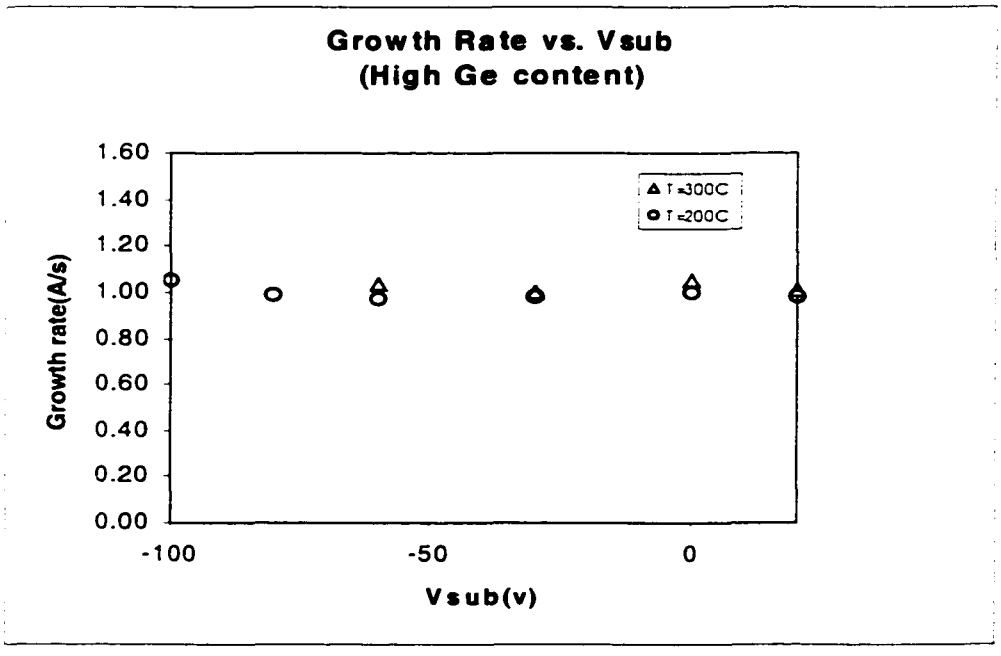

Figure 4.8 Growth rate vs. Substrate biasing for high Ge content films

The effects of hydrogen dilution and temperature are also shown in Figure 4.6 and 4.7. From Figure 4.6, when substrate bias increases, the growth rate for the low temperature also increases, but not as fast as the one at high temperature. It is because that at low temperature, the surface mobility is low and more ion bombardment is needed to increase the growth rate. Figure4.7 shows the growth rate vs. substrate bias under different hydrogen dilution. The growth rate keeps increasing with negative substrate bias. The effect of the substrate bias at low hydrogen dilution is not as strong as that at high hydrogen dilution. It is because that hydrogen homogenizes the surface and etches the surfaces (exothermic reaction), so ion bombardment becomes more effective at the high hydrogen dilution.

4.2.3.2 The effect of substrate bias on α-(Si,Ge):H device

Some reports have studied the effects of dc bias on properties of amorphous silicon films and their alloys [24-26]. The effects of ion bombardment are determined by both the ion flux density and the bombardment energy of the incident ions. In the ECR PECVD process, by using negative DC bias method, both the ion bombardment energy and the ion flux are increased (Mathew DeFreese's thesis[42]). The ion energy is defined by (V_s-V_{dc}), where Vs is the plasma space potential.

Some samples have been grown under different substrate biasing. Deposition parameters are shown in Table 4.6. Thickness, I-V curve, Tauc gap, Urbach energy and Quantum efficiency are measured as mentioned before. The results are shown in Figure 4.9.-4.13.

From Figure 4.9-4.13, it is shown that E_{tauc} increases, V_{oc} increases, FF increases and $\mu\tau$ decreases with the increasing negative biasing. The substrate voltage makes Ge grow more homogeneously because of the greater ion bombardment, while the Ge-Ge cluster will lead to an apparently lower bandgap. So the more homogeneous film will also lead to higher bandgap. V_{oc} is increasing when a negative voltage is applied, which is consistent with E_{tauc} data.

Table 4.6: Deposition parameters for α-(Si,Ge):H films

	Temperature	Pressure	Power	H2(%)	SiH4(%)	GeH4(%)	TMB(%)
Group 1	360°C	15 mTorr	123 W	100	15	30	20
Group 2	360°C	15 mTorr	123 W	100	15	40	20
Group 3	300°C	15 mTorr	123 W	60	15	40	20
Group 4	360°C	15 mTorr	150 W	60	15	30	20
Group 5	300°C	10 mTorr	123 W	60	15	40	20

Fill factor is also higher for negative biasing. There are two possible reasons to explain this situation. The first is, as we mentioned before, Ge-Ge clusters are broken, the film grows more homogeneously. The second is that the greater ion bombardment suppresses dyhidride bonds. Both make the defect density decrease, so the hole diffusion length increases, so FF increases. These data are consistent with the data on E_{ur} and $\mu\tau$ product of holes shown in Figure 4.12 and 4.13.

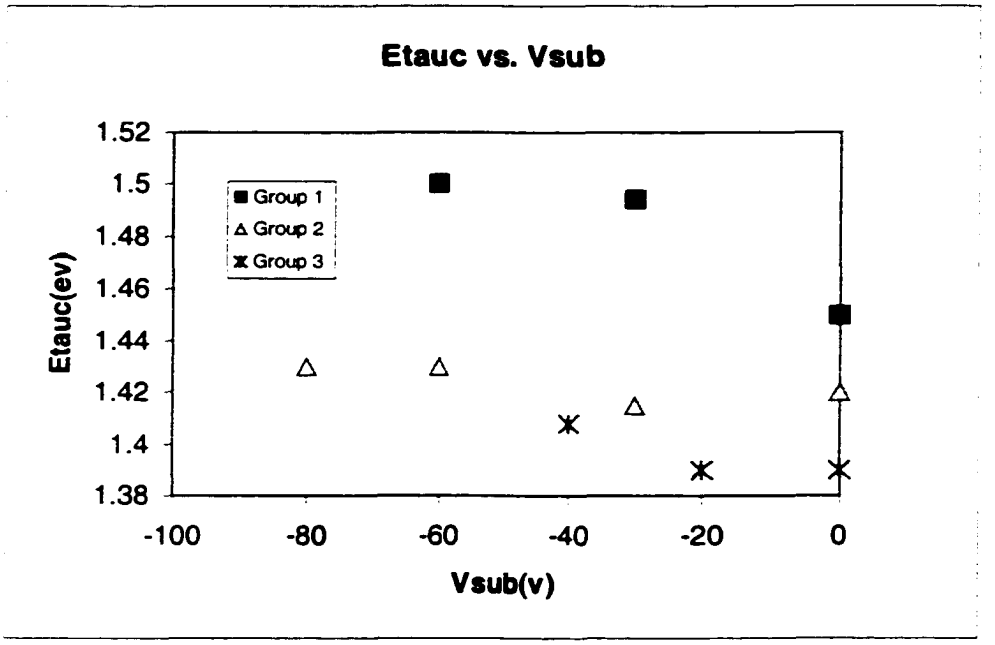

Figure 4.9 Tauc gap vs. Substrate bias

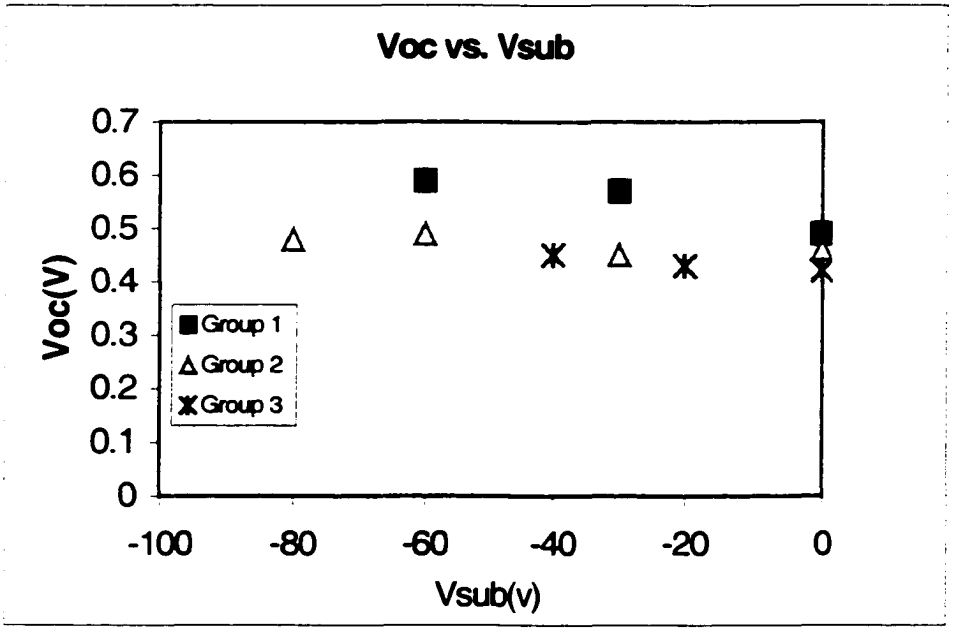

Figure 4.10 Voc vs. Substrate bias

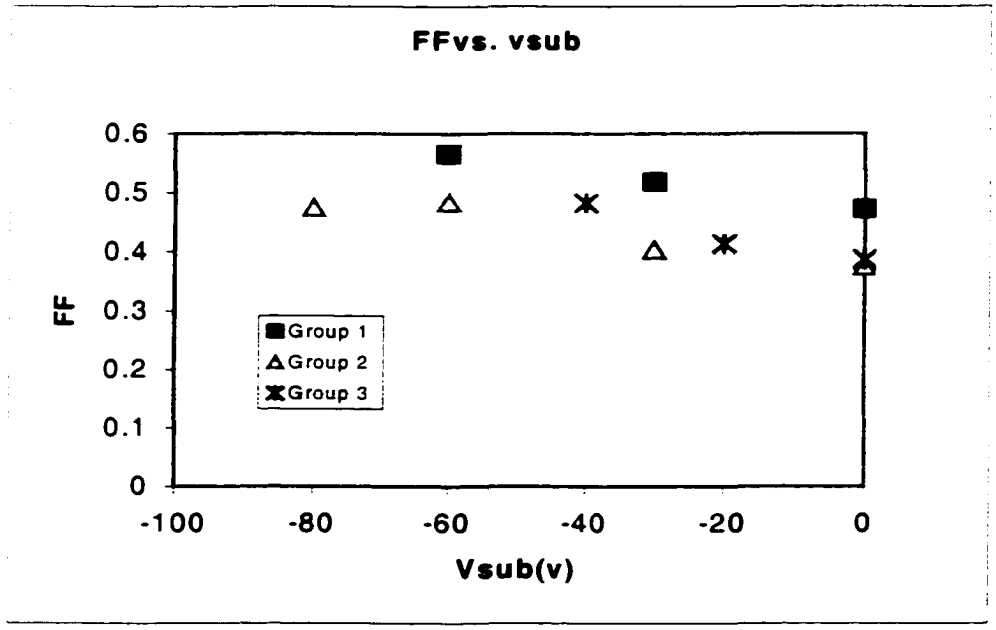

Figure 4.11 Fill factor vs. Substrate bias

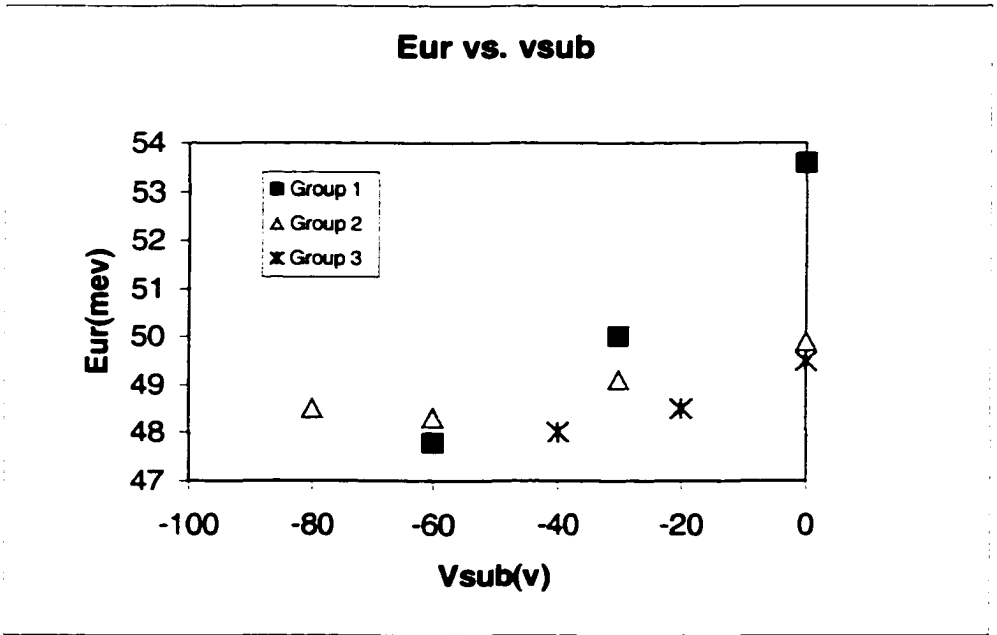

Figure 4.12 E_{ur} vs. Substrate bias

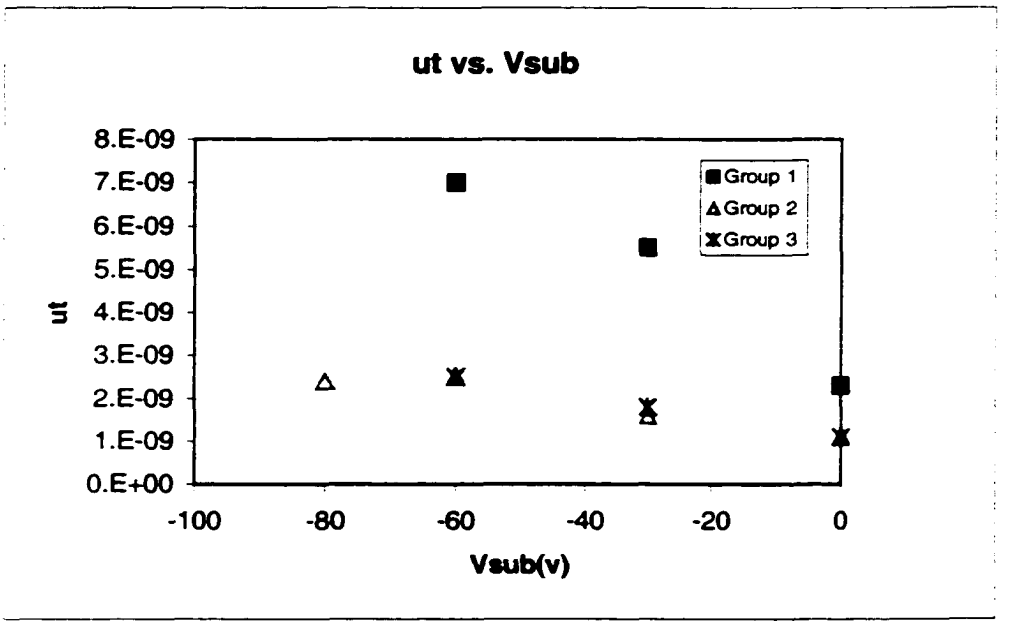

Figure 4.13 Hole mobility lifetime product vs. Substrate bias

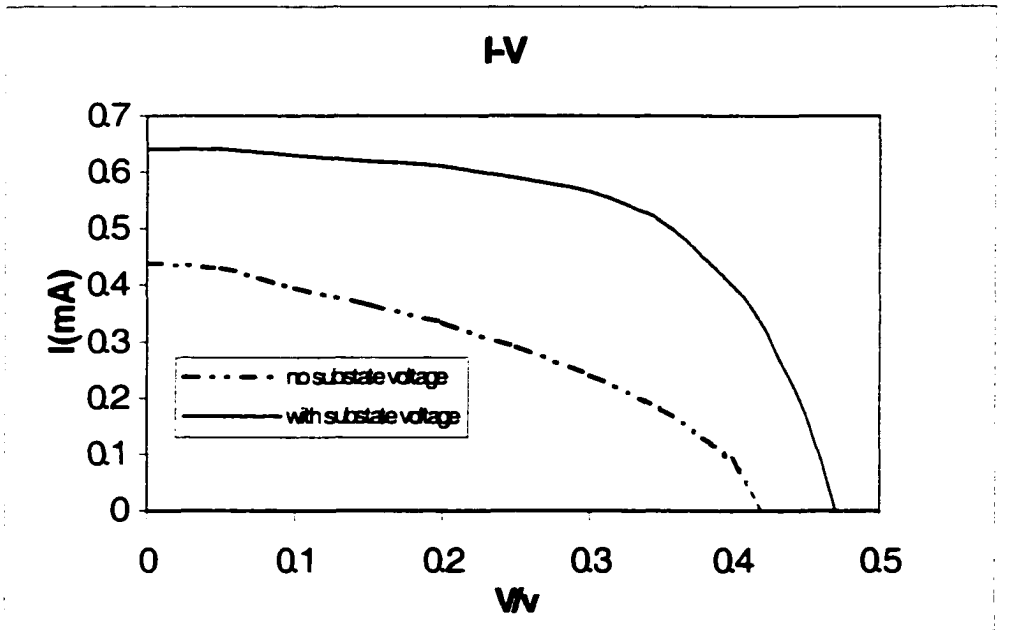

Figure 4.14 I-V curves for two samples with and without substrate bias

The Urbach energy decreases when substrate voltage is increasing, which is a signature of decreasing disorder. It shows that the defect density decreases, which means the film is grown more homogeneously when substrate voltage is applied. $\mu\tau$ data is increasing with negative dc bias, which is consistent with less disorder.

Figure 4.14 shows the I-V curves for two samples with and without substrate bias. We can see that the V_{oc}, I_{sc} and fill factors are much improved by applying the substrate bias. The fill factor even increases by more than 20%.

In conclusion, under certain deposition environments, the quality of devices is improved when negative substrate voltage is applied. But when the pressure is low and the power is high, the ion bombardment is already strong enough and then the effect of substrate bias is weak. For example, the substrate voltage did not show any improvement on device quality for Group 4 and Group 5.

4.3 Low bandgap α-(Si,Ge):H and α-(Ge):H devices

It's generally believed that the quality of the material and device degrades significantly as the Ge content increases, with alloys having >50% Ge content being rather poor in quality. High quality p-i-n devices have been made and studied for Ge content <50% in most of the research [5-9]. However, only a few investigations [7][23] have been done for films of Ge content >50%, and fewer still on devices. In this report, we explored the properties of α-(Si,Ge):H alloys with Ge content <50% for both films and devices under the combination of high temperature, high hydrogen dilution and ion bombardment.

4.3.1 Films

First, some films are deposited on Corning 7059 glass. The growth precursors are silane and germane or germane alone. The films are grown with a high hydrogen dilution (>20:1) and low pressure (≤10mT) with high temperature (≥.300°C) The deposition parameters are shown in Table 4.7, including samples with different SiH4/GeH4 ratios, different hydrogen dilutions and different temperatures. When the target pressure is 5 mTorr, the real pressure of these samples is between 5mTorr and 6 mTorr because of the limitation of the system.

The electrical and optical properties are investigated by the Tauc gap, Urbach energy and photo/dark conductivity measurements, which are shown in Table 4.8.

Table 4.7: Deposition parameters for low bandgap α-(Si,Ge):H and α-(Ge):H films

	Temperature	Pressure	Power	H2(%)	SiH4(%)	GeH4(%)	TMB(%)
2/4396	350°C	5 mTorr	150 W	60	5	100	20
2/4394	350°C	5 mTorr	150 W	60	6	90	20
2/4400	350°C	5 mTorr	150 W	60	8	80	20
2/4393	350°C	5 mTorr	150 W	60	10	90	20
2/4333	350°C	5 mTorr	150 W	80	5	90	20
2/4334	350°C	5 mTorr	150 W	80	6	60	20
2/4405	350°C	10 mTorr	150 W	60	0	60	20
2/4406	300°C	10 mTorr	150 W	60	0	60	20
2/4397	300°C	5 mTorr	150 W	60	0	100	20

From the results, the Tauc gap variation is from 1.03 eV to 1.42 eV because of the different SiH4/GeH4 ratios. Figure 4.15 shows photo and dark conductivity vs. Tauc gap. Figure 4.16 shows photoconductivity /dark-conductivity ratio vs. Tauc gap. Figure 4.17 shows Urbach energy vs. Tauc gap.

Table 4.8: Results for low bandgap α-(Si,Ge):H and α-(Ge):H films

	E_{tauc}(eV)	E_{04}(eV)	E_{ur}(meV)	σ_L(S/cm)	σ_D(S/cm)	σ_L/σ_D
2/4396	1.25	1.41	41	3.72e-6	6.16e-8	6.04e01
2/4394	1.31	1.44	50	6.87e-6	6.23e-8	1.10e02
2/4400	1.32	1.47	42	5.68e-6	4.37e-8	1.30e02
2/4393	1.34	1.46	47	1.00e-6	4.62e-9	2.17e02
2/4333	1.33	1.43	55.7	4.42e-6	5.83e-8	7.57e01
2/4334	1.42	1.55	46	6.35e-6	1.1e-8	5.77e02
2/4405	1.08	1.21	48	6.29e-5	5.24e-5	1.20e00
2/4406	1.03	1.23	41	2.89e-4	2.24e-4	1.29e00
2/4397	1.06	1.21	48	4.49e-4	3.55e-4	1.26e00

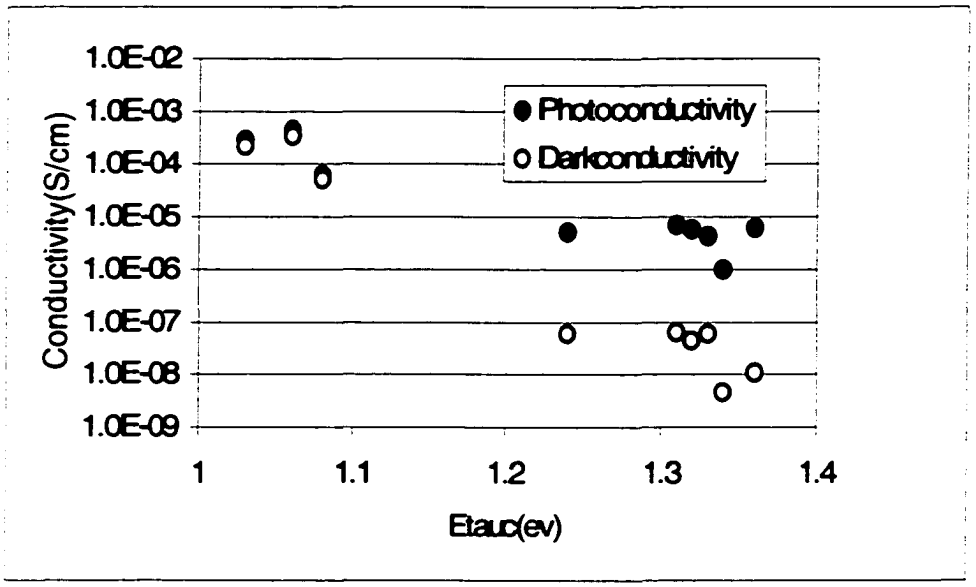

Figure 4.15 Photo and dark conductivity vs. Tauc gap

From Figure 4.15 and 4.16, we find that the photoconductivity decreases, dark conductivity decreases, but σ_L/σ_D increases with increasing Tauc gap. From Figure 4.17, E_{ur} doesn't change much with Tauc gap. The values of Eur are low for such a high Ge content. The typical Urbach energy curve with E_{tauc}=1.25 eV is also shown in Figure 4.18, which is about 40-42 meV.

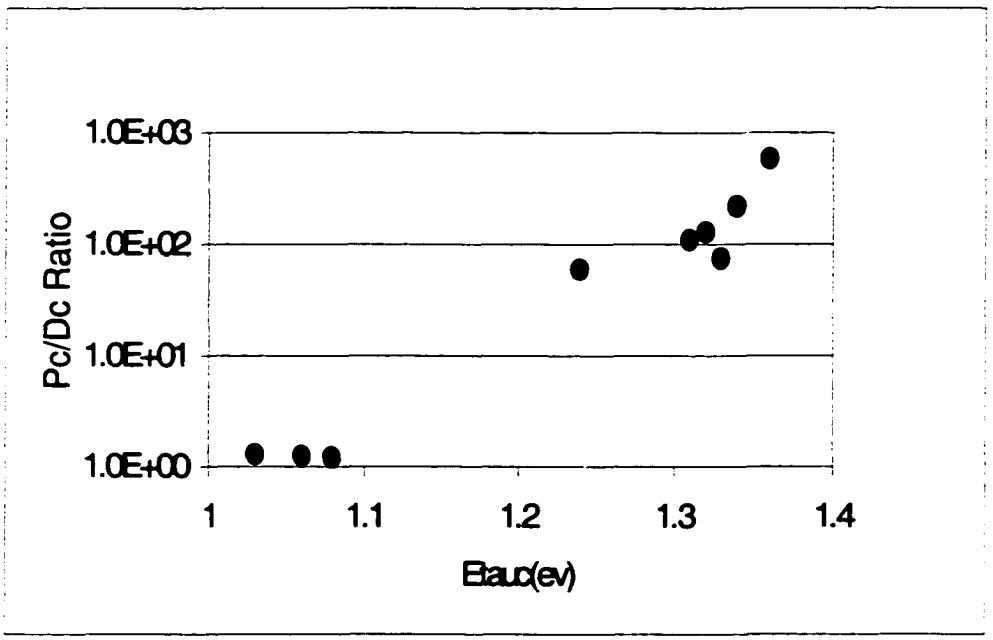

Figure 4.16 Photo-conductivity/dark-conductivity vs. Tauc gap

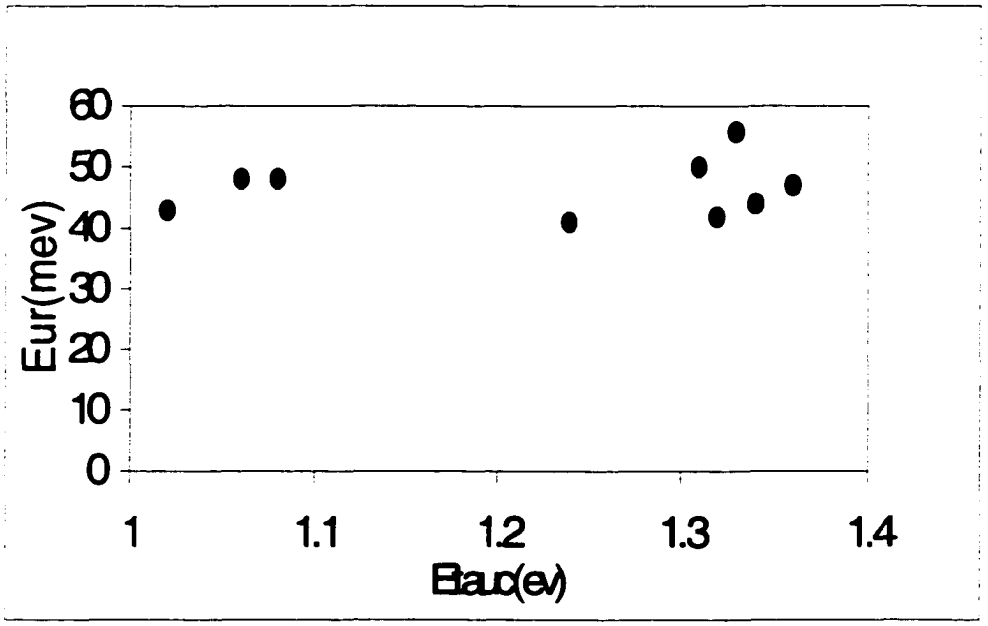

Figure 4.17 Urbach energy vs. Tauc gap

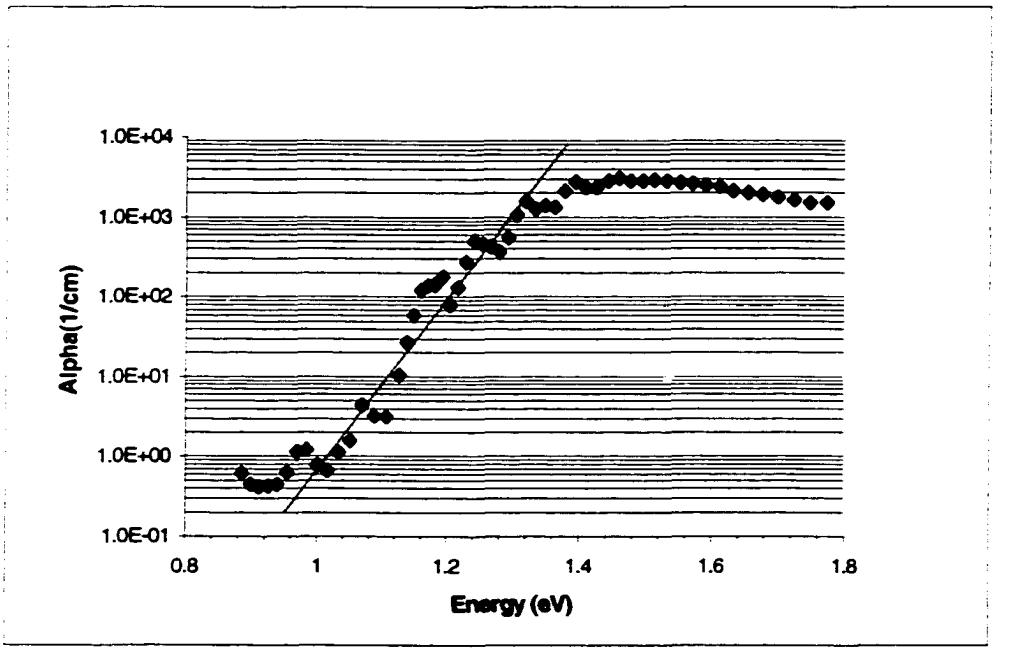

Figure 4.18. The Urbach energy of 1.25 eV cell

4.3.2 Devices

Some devices are grown on stainless steel with similar deposition parameters to those films. The thickness of the i layer is about 0.15-0.2 μm and the growth rate is about 1 Å/s. The TMB is graded from 0% to 40% from the n side to the p side. The deposition parameters are shown in Table 4.9. The results of these samples are shown in Table 4.10.

When the Tauc gap varies from 1.16 eV for pure α-(Ge):H device to 1.34 eV for α-(Si,Ge):H device, the open circuit voltage increases from 0.34 V to 0.52 V. The fill factor varies from 51% to 61% except for the one deposited at low temperature. The

Urbach energy is between 40-50 meV. These values are very good for such a low bandgap device.

Figure 4.19 and 4.20 show the I-V curve for E_{tauc}=1.34 eV and E_{tauc}=1.16 eV. The fill factors for the two cells are 61% and 51% respectively. Figure 4.21 and 4.22 show the QE and QE ratio plot across the photon spectrum for the two samples separately. The low ratio is an indication of the good collection of both electrons and holes although not as good as the best α-(Si):H devices. Figure 4.23 and 4.24 show that the defect density of states of the two cell. The defect density for the 1.34 cell is about 6e16 $cm^{-3}eV^{-1}$ and that for the 1.16 cell is 2e1 $cm^{-3}eV^{-1}$.

Table4.9: Deposition parameters for low bandgap α-(Si,Ge):H and α-(Ge):H devices

	Temperature	Pressure	Power	H2(%)	SiH4(%)	GeH4(%)	TMB(%)
2/4307	350°C	5 mTorr	150 W	80	6	60	0-40
2/4308	350°C	5 mTorr	150 W	80	6	70	0-40
2/4322	350°C	5 mTorr	150 W	80	5	50	0-40
2/4321	350°C	5 mTorr	150 W	80	5	70	0-40
2/4324	350°C	5 mTorr	150 W	80	5	90	0-40
2/4310	350°C	5 mTorr	150 W	70	5	90	0-40
2/4360	350°C	5 mTorr	150 W	80	0	60	0-40
2/4327	300°C	5 mTorr	150 W	80	5	90	0-40

Table 4.10: Results for low bandgap α-(Si,Ge):H and α-(Ge):H devices

	V_{oc}(V)	I_{sc}(mA)	FF	E_{ur}(meV)	E_{tauc}(eV)
2/4307	0.52	0.64	61.10%	45.0	1.34
2/4308	0.52	0.58	58.80%	43.0	1.31
2/4322	0.49	0.80	54.20%	42.0	1.32
2/4321	0.49	0.74	59.60%	46.0	1.30
2/4324	0.43	0.95	52.50%	45.6	1.24
2/4310	0.44	0.50	58.00%	47.7	1.27
2/4360	0.34	0.87	51.00%	40.0	1.16
2/4327	0.51	0.65	43.80%	45.7	1.35

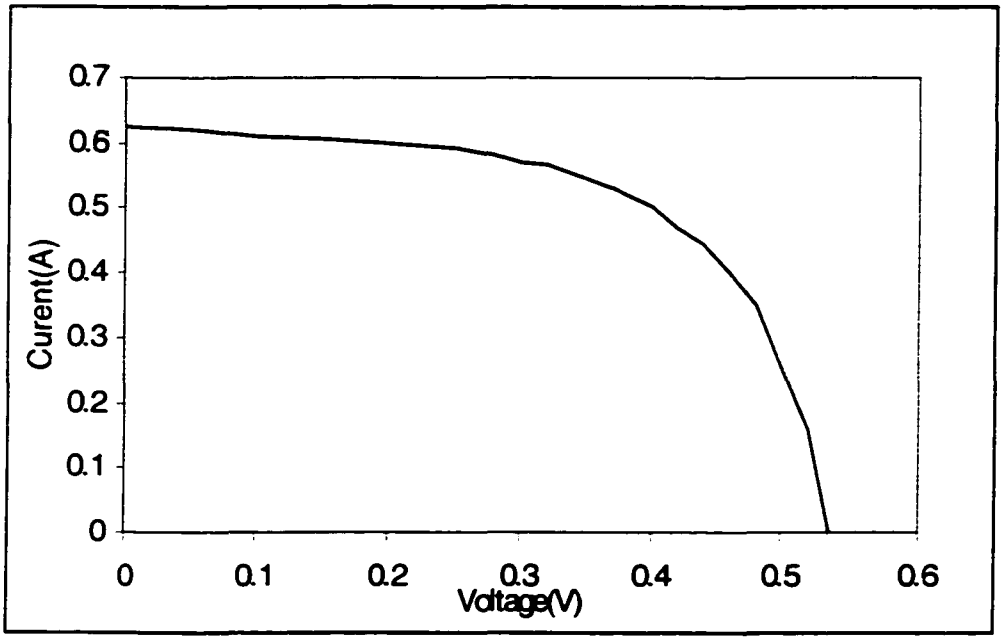

Figure 4.19 I-V curve for 1.34 eV cell

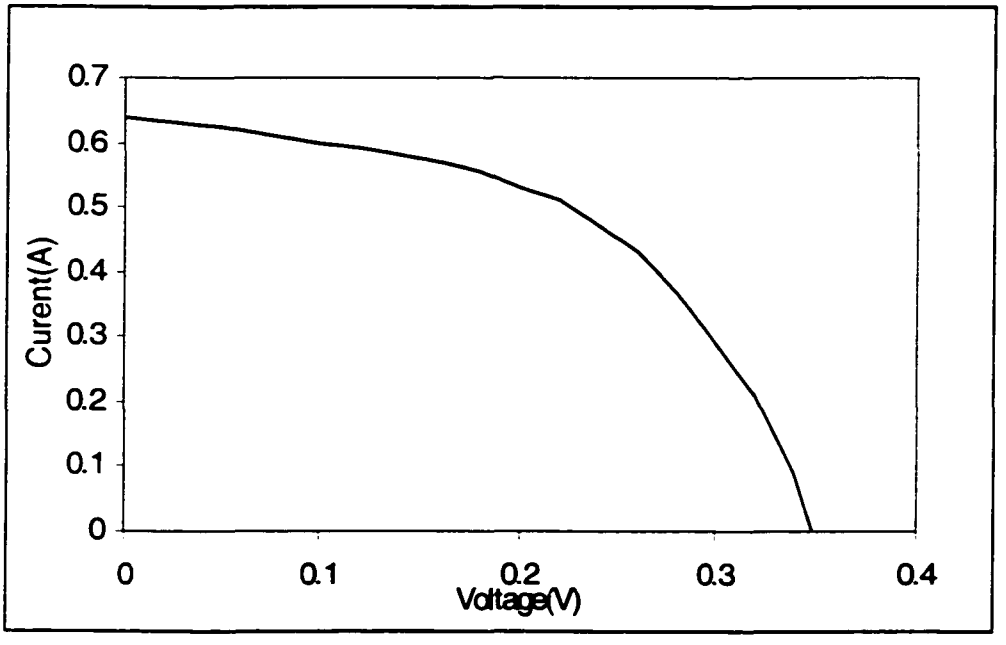

Figure 4.20 I-V curve for 1.16 eV cell

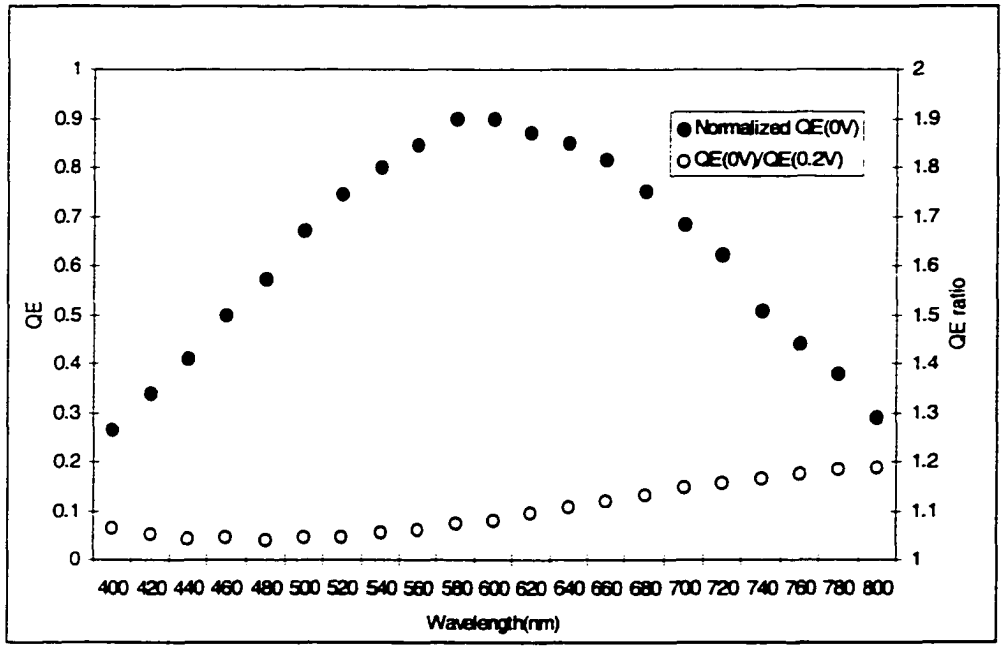

Figure 4.21 QE and QE ratio for 1.34 eV cell

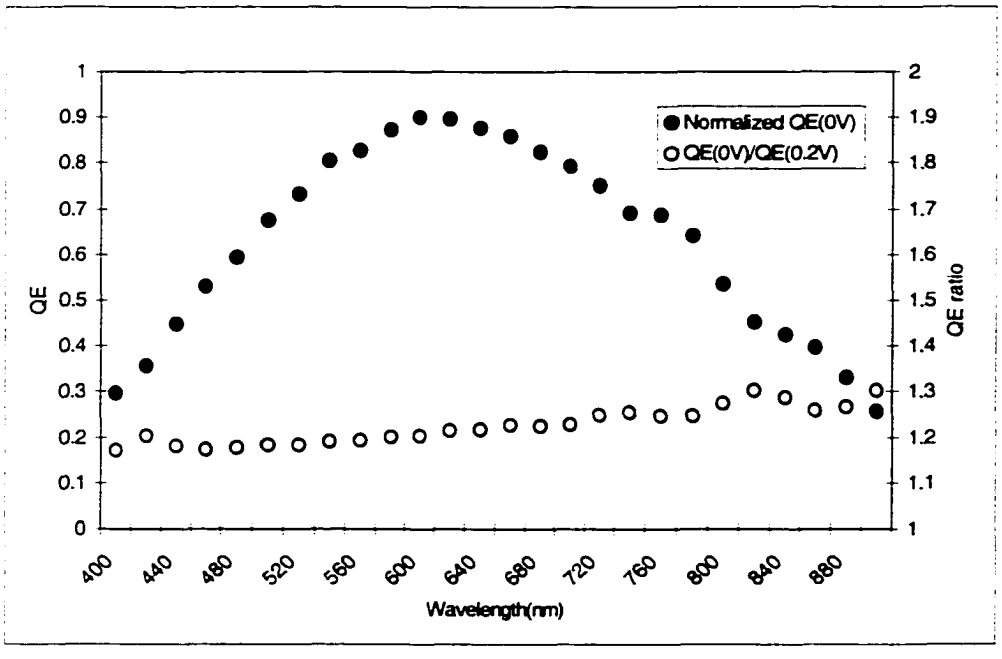

Figure 4.22 QE and QE ratio for 1.16 eV cell

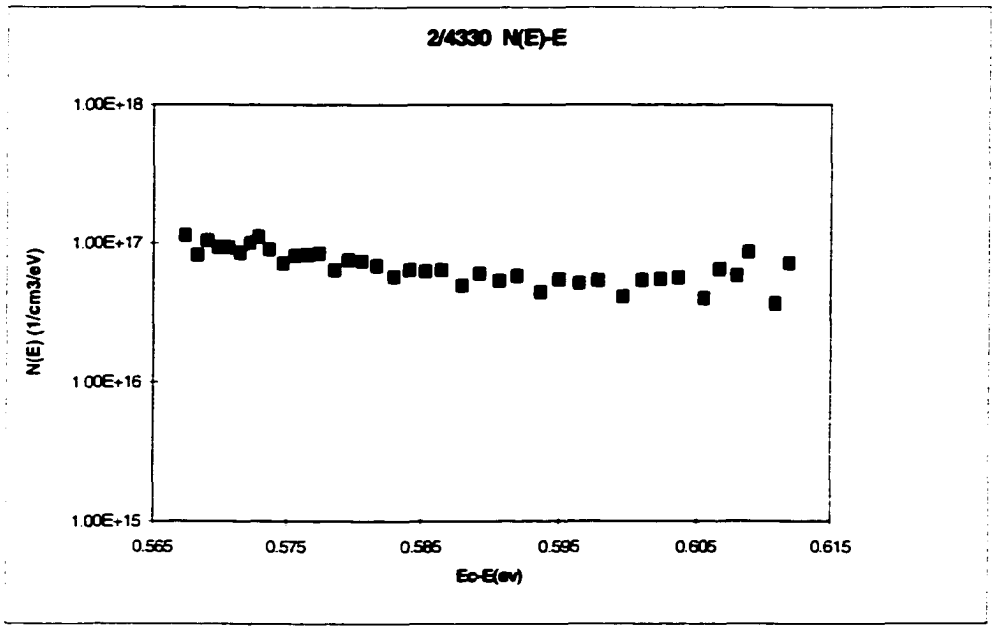

Figure 4.23 Defect density for 1.34 eV cell

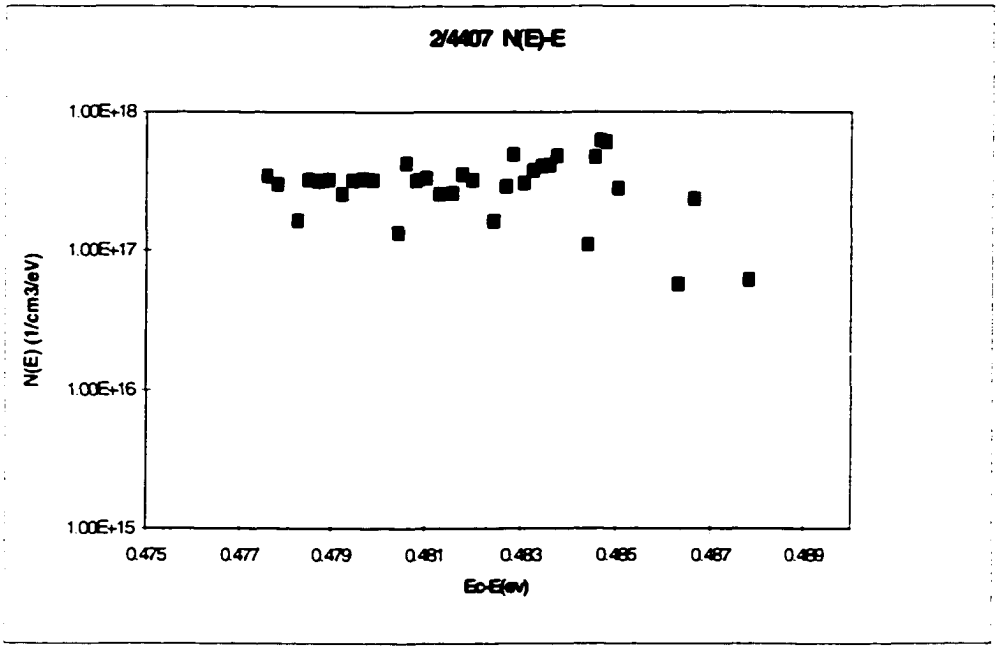

Figure 4.24 Defect density for 1.16eV cell

4.3.3 FTIR measurements

To make FTIR measurements, some samples are deposited on the double side polished silicon wafer. Two are α-(Si,Ge):H samples deposited at different pressures while other parameters are almost the same. The third sample is pure α-(Ge):H. The deposition parameters are shown in Table 4.11.

Table 4.11 Deposition parameters for α-(Si,Ge):H and α-(Ge):H films

	Temperature	Pressure	Power	H2(%)	SiH4(%)	GeH4(%)	TMB(%)
2//4401	350°C	5.6 mTorr	150 W	60	6	90	20
2//4402	350°C	10 mTorr	150 W	60	5	80	20
2//4403	350°C	10 mTorr	150 W	60	0	60	20

Figure 4.25 and 4.26 show the FTIR results of two samples made at different pressure. The spectrum has big fluctuations which is resulting from the difference of the reflective index of the Si wafer and the low bandgap α-(Si,Ge):H material. The characteristic peaks are located on this interference background, which limits the accurate measurement of the hydrogen content to only some qualitative analysis. The high pressure sample has peaks at 2150 cm^{-1}, 2020cm^{-1}, 1890 cm^{-1}, 618 cm^{-1}, 580 cm^{-1}. They are $(SiH_2)_n$ bond stretching mode, Si-H bond stretching mode, Ge-H bond stretching mode, Si-H bond bending mode and Ge-H bond bending mode respectively. The Si-H bond stretching mode shifted slightly from 2000 cm^{-1} to 2020 cm^{-1} because of the existence of the $(SiH_2)_n$ bond. The low pressure sample also has corresponding peaks at 2007 cm^{-1}, 1890 cm^{-1}, 630 cm^{-1}, 580 cm^{-1}. There is another peak at 1110 cm^{-1}, which is the Si-O surface bond. Comparing the two spectra, we can find that the $(SiH_2)_n$

bond is not obvious in the spectrum of the low pressure sample. So the ion bombardment helps to break up the poly Si-H_2 bond, which is consistent with the result obtained by S. Sugiyama and J.Yang [26].

Another important result is that the preference of Si-H to Ge-H was broken up by ion bombardment. FTIR results shows that the relative amplitude of the peaks for both the Ge-H bond stretching mode and bending mode to Si-H bond stretching mode and bending mode for the low pressure sample is much higher than those of the high pressure sample. From Chapter 1, we know that the preferential attachment of hydrogen to silicon rather than Germanium is the one of the major reasons that α-(Si,Ge):H alloys have more defect density and have poorer opto-electrical properties than α-Si:H.

This result is also consistent with our previous assumption [27] that the higher ion bombardment at low pressure reduces Ge-Ge clusters and make the film grows more homogeneously. The increasing concentration of Ge-H bonds verified the decreasing Ge-Ge cluster density indirectly.

The FTIR spectrum of the pure α-(Ge):H is shown in Figure 4.27, which has a Ge-H stretching bond at 1890 cm^{-1} and bending bond at 580 cm^{-1}.

Si-H_2 and GeH_2 stretching bond and bending bond are not obvious except in the first spectra, which shows that the Si-H and Ge-H bonds are predominant in the material grown in the ECR PECVD system under optimal plasma conditions.

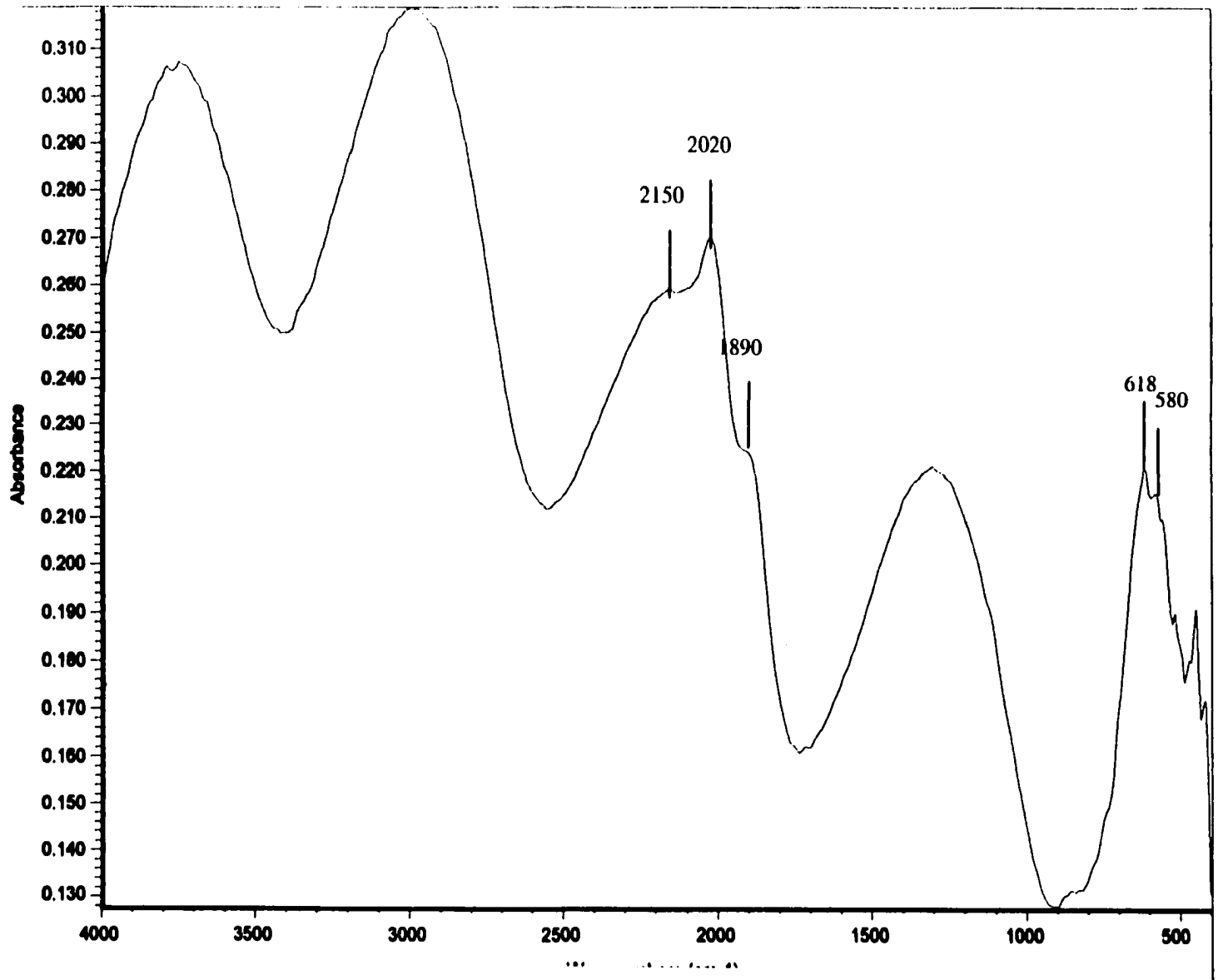

Figure4.25 FTIR spectrum for high pressure sample

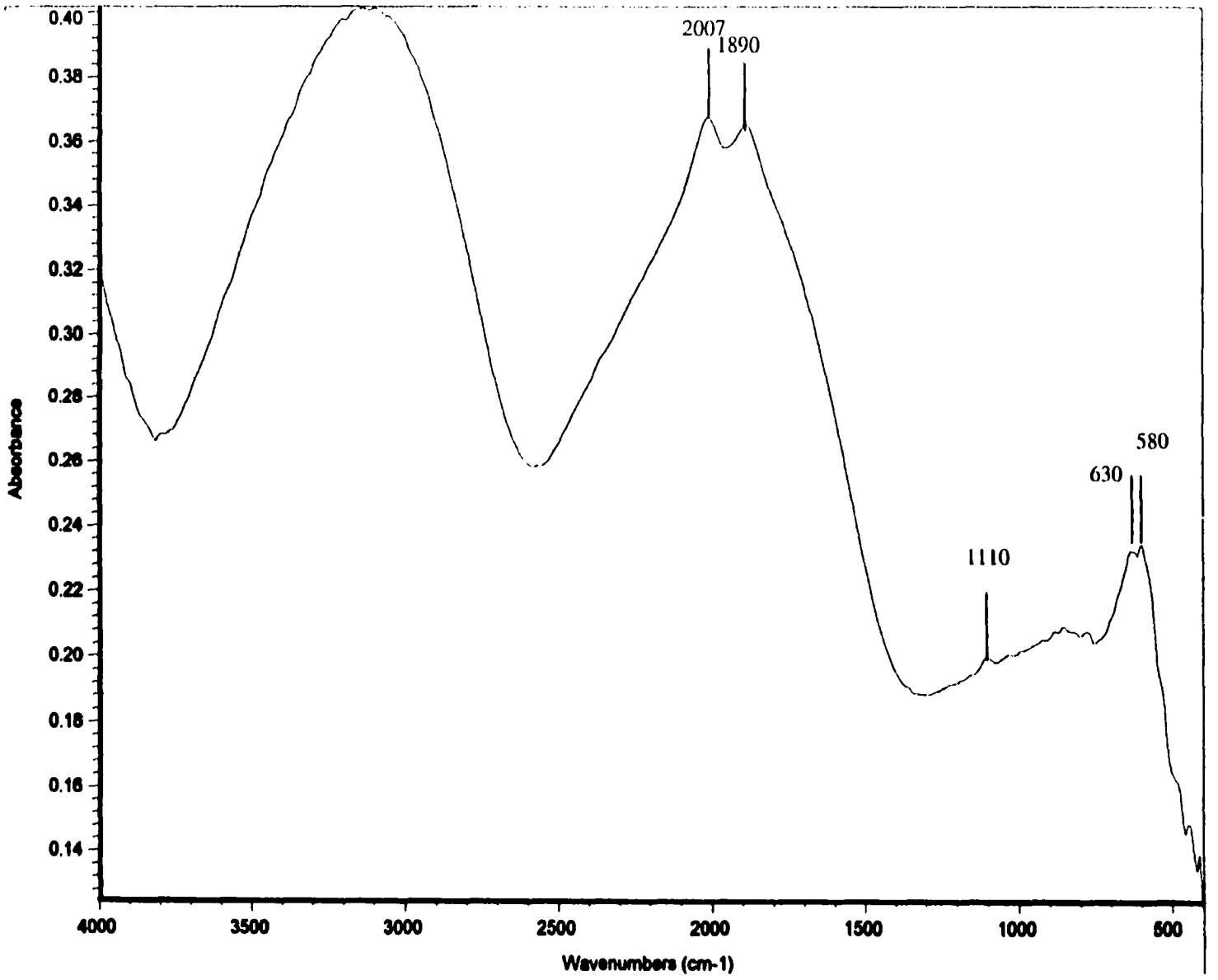

Figure4.26 FTIR spectrum for low pressure sample

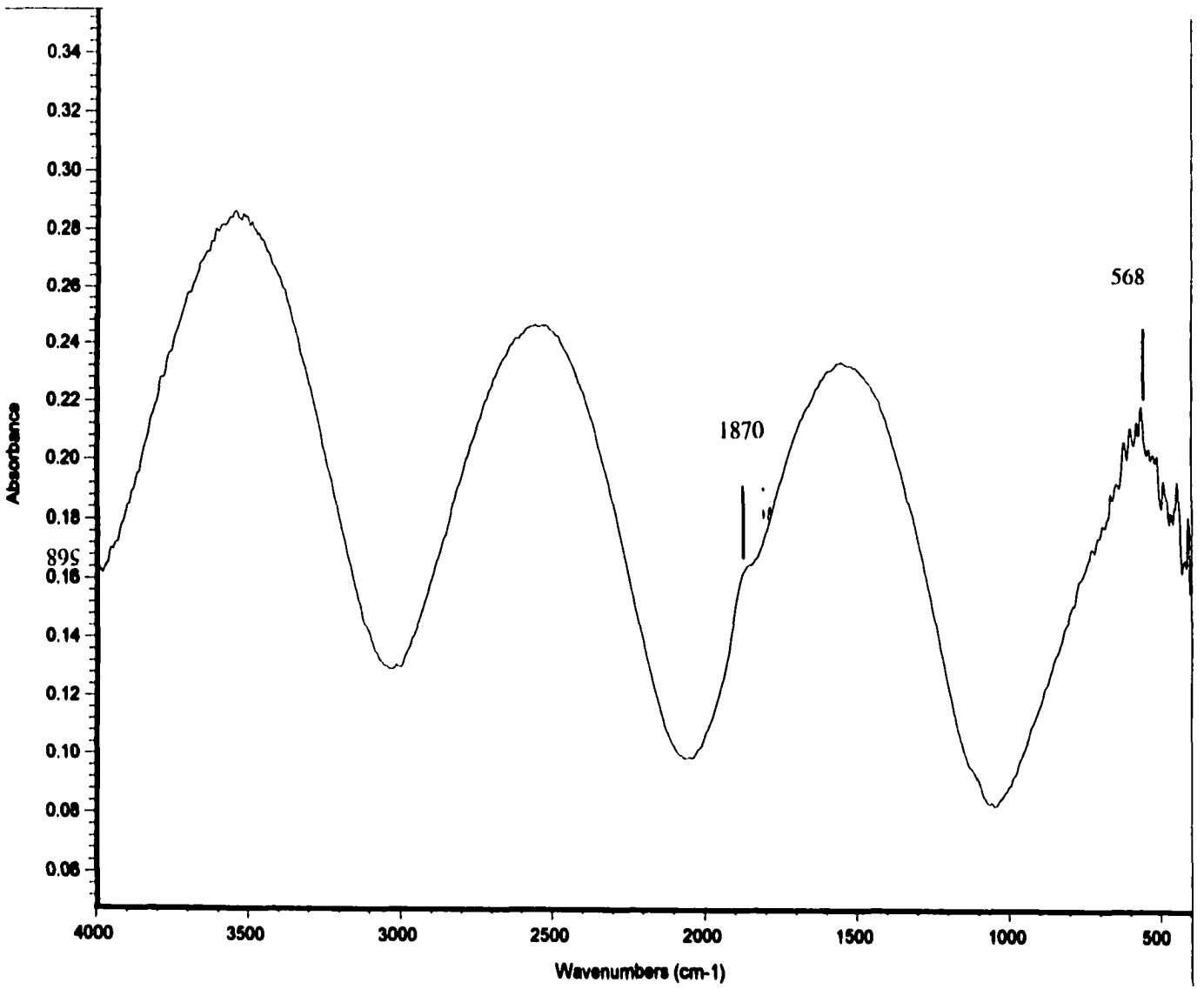

Figure4.27 FTIR spectrum for amorphous germanium sample

4.3.4 Further improvement of α-(Si,Ge):H and α-(Ge):H devices

According the previous results we obtained, substrate bias and ppm boron doping are used to further improve the performance of the devices.

4.3.4.1 Substrate bias

Some α-(Si,Ge):H and α-(Ge):H samples are deposited under substrate bias from 0 V to –90 V. The deposition parameters are shown in Table 4.12-13 and results in Table 4.14-15.

Table 4.12 Deposition parameters for α-(Si,Ge):H with varying substrate bias

	Vbias	Temperature	Pressure	Power	H2(%)	SiH2(%)	GeH4(%)	TMB(%)
2//4294	0 V	350°C	10 mTorr	150 W	100	7	100	0-48
2//4295	-30 V	350°C	10 mTorr	150 W	100	7	100	0-48
2//4296	-60 V	350°C	10 mTorr	150 W	100	7	100	0-48
2//4297	-90 V	350°C	10 mTorr	150 W	100	7	100	0-48

Table 4.13: Results for α-(Si,Ge):H with varying substrate bias

	V_{oc}(V)	I_{sc}(mA)	FF	E_{ur}(meV)	E_{tauc}
2//4362	0.46	0.51	50.80%	46.8	1.28
2//4364	0.42	0.78	52%	44.4	1.28
2//4360	0.44	0.67	56.80%	42	1.28
2//4361	0.43	0.74	48.80%	40	1.28

Table 4.14 Deposition parameters for α-(Ge):H with varying substrate bias

	Vbias	Temperature	Pressure	Power	H2(%)	GeH4(%)	TMB(%)
2//4335	0 V	350°C	5 mTorr	150 W	80	60	0-25
2//4337	-30 V	350°C	5 mTorr	150 W	80	60	0-25
2//4338	-60 V	350°C	5 mTorr	150 W	80	60	0-25
2//4339	-90 V	350°C	5 mTorr	150 W	80	60	0-25

Table 4.15: Results for α-(Ge):H with varying substrate bias

	V_{oc}(V)	I_{sc}(mA)	FF	E_{ur}(meV)	E_{tauc}
2//4335	0.35	0.66	49%	44	1.14
2//4337	0.34	0.64	52%	40	1.17
2//4338	0.33	0.46	55%	38	1.18
2//4339	0.34	0.7	47%	46	1.16

Figure 4.28 shows the fill factor vs. substrate bias and Figure 4.29 shows the E_{ur} vs. substrate bias. We can see that the two data are self-consistent and substrate bias can provide some ion bombardment to improve the quality of the materials when substrate bias > -60 V. But when the ion bombardment is too strong (substrate bias < -60 V), the quality of the films degrades. Another thing is that for α-(Ge):H devices, high ion bombardment still has effects even under low pressure. It is because of the fact that the mobility of the germyl is small. It's different from the alloy.

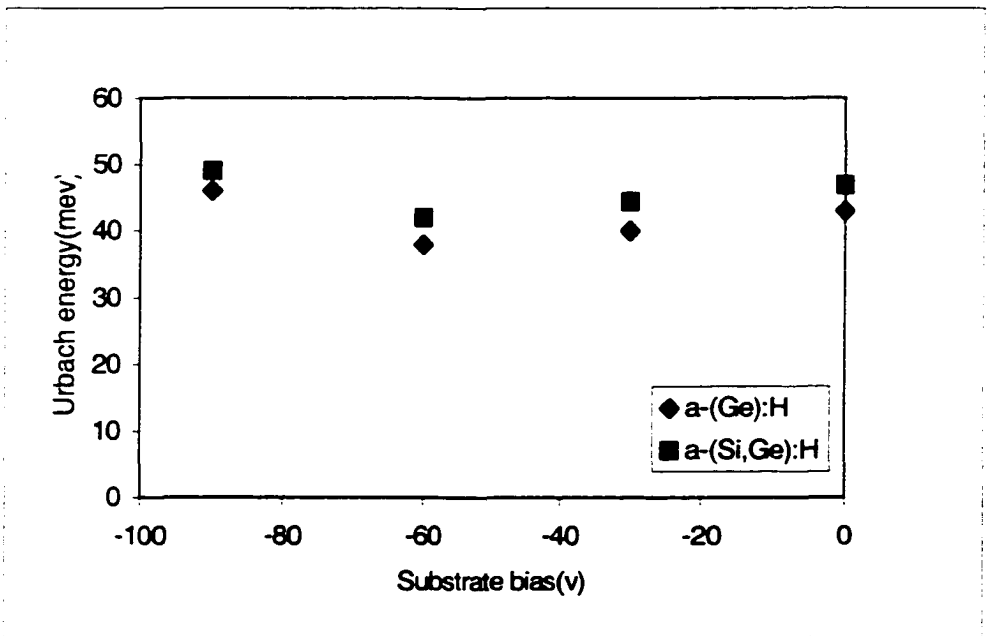

Figure 4.28 Urbach energy vs. substrate bias

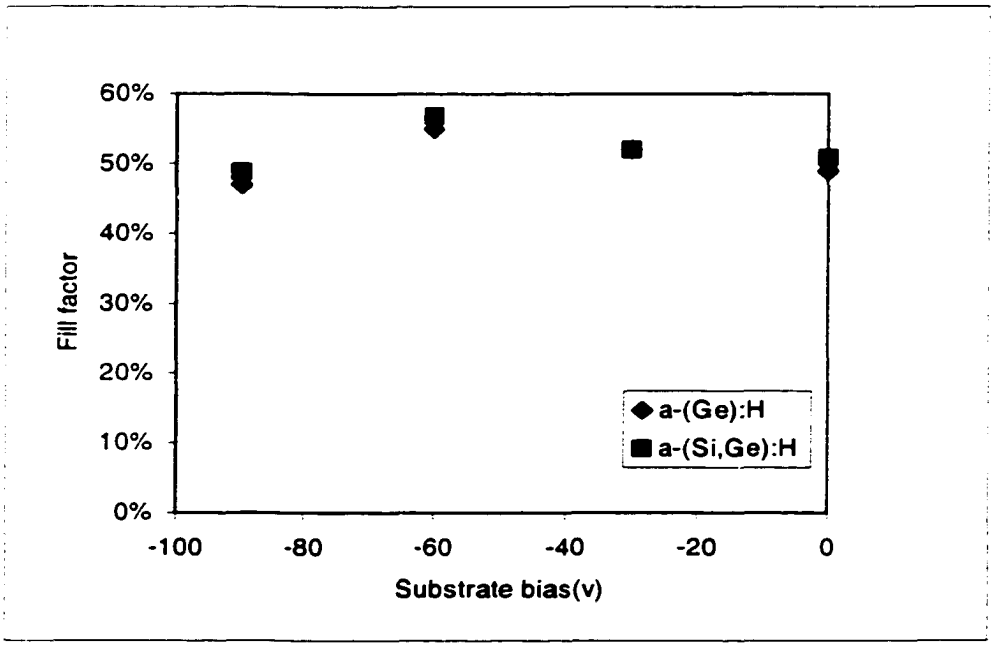

Figure 4.29 Fill factor with different substrate bias

4.3.4.2 Graded boron doping in i layer

Some pure α-(Ge):H samples are deposited under different ppm boron doping. The ppm boron doping is graded increasingly from the n side to the p side. The deposition parameters are shown in Table 4.16. The results are shown in Table 4.17.

The ppm boron doping can compensate the oxygen incorporated into the i layer from the environment. We can see that the addition of ppm boron doping improved the performance of the device, which is shown by the value of fill factor and Urbach energy. But when the boron doping reaches some value, the quality of the films degrades.

Table 4.16 Deposition parameters for α-(Ge):H with varying boron doping in i layer

	Temperature	Pressure	Power	H2(%)	GeH4(%)	TMB(%)
2//4362	350°C	5 mTorr	150 W	80	60	0
2//4364	350°C	5 mTorr	150 W	80	60	0-20
2//4360	350°C	5 mTorr	150 W	80	60	0-40
2//4361	350°C	5 mTorr	150 W	80	60	0-60

Table 4.17: Results for α-(Ge):H with varying boron doping in i layer

	V_{oc}(V)	I_{sc}(mA)	FF	E_{ur}(meV)	E_{tauc}
2//4362	0.34	0.715	46%	45	1.15
2//4364	0.36	0.78	49%	43	1.18
2//4360	0.34	0.875	51%	40	1.16
2//4361	0.35	0.84	45%	46	1.17

CHAPTER 5. CONCLUSION

In this research, α-(Si,Ge):H and α-(Ge):H devices are grown by electron cyclotron resonance plasma enhanced CVD technique and the electrical and optical properties of these devices under different plasma conditions are investigated.

The ion bombardment during growth can be enhanced by low pressure, inert gas and substrate bias. The conclusion that low pressure leads to better quality of the material under hydrogen plasma because of higher ion bombardment is further verified by the space charge limited current (SCLC) method. The midgap defect density of states for the low pressure sample is lower than the one deposited under high pressure. The resulting density of states for samples at 5 mTorr is only about $2*10^{16}/cm^3$. Unlike the case for hydrogen plasma, the film properties for He-ECR films did not degrade as the pressure changed from 10mTorr to about 25 mTorr. however, the film properties degrade at higher pressure (35 mTorr). It's because the ion energy of He plasma is higher than that of H plasma.

We also found that negative substrate bias can provide higher ion bombardment. The effects of substrate bias on the growth rate are different for the high Ge content sample and the low Ge content sample. At the low Ge content, growth rate increases with increasing of negative substrate bias. At high Ge content, growth rate keeps constant with the substrate bias. At low temperature and low hydrogen dilution, we found that more ion bombardment are needed to increase the growth rate. Under certain

deposition environments, the performance of the devices can be improved when negative substrate voltage is applied. But under some conditions such that the ion bombardment is already high, the effect is not so obvious.

The quality of the material and device degrades significantly as the Ge content increases, with alloying having >50% Ge content being rather poor in quality. High quality p-i-n device have only been made for Ge contents <50%. In this work, we explored the properties of α-(Si,Ge):H alloys with Ge contents <50% and found that device quality material can be obtained under the combination of low pressure, high temperature, high hydrogen dilution and ppm boron doping in the i layer even for a bandgap as low as 1.16 eV.

Fourier transformed infrared absorptance spectroscopy (FTIR) measurement showed that the density of the $(SiH_2)_n$ bond was reduced by the ion bombardment at low pressure. Another important result by FTIR is that the preference of Si-H to Ge-H is broken up, low pressure and high hydrogen dilution is beneficial to increase the density of Ge-H bond. The increases of the density of the Ge-H bond leaded to less Ge dangling bond and Ge-Ge cluster so that the material is grown more homogeneously.

The performance of the low bandgap α-(Ge):H and α-(Ge):H devices could be further improved by providing some graded boron doping in i layer and negative substrate bias. A fill factor of 55% and Urbach energy of about 40 meV were obtained for an α-(Ge):H solar cell. This is the first time ever that a good α-(Ge):H solar cell has been made.

At last, more future work on ion bombardment, particularly momentum effects by using Ar +H_2, needs to be done because that Ar can help in momentum transfer and H_2 can help chemical reactions and surface homogenization. The combination of both may improve the quality of the device. And also more work on α-Ge:H because the material is still not as good as α-Si:H.

REFERENCES

1. W. Luft and Y. Tsuo, Hydrogenated Amorphous Silicon Alloy Deposition Processes, Marcel Dekker, Inc., New York, 1993
2. J. Ho, Y. Fang, K. Wu and S. Tsai, "High-gain p-I-n infrared photosensors with Bragg reflectors on amorphous silicon-germanium alloy", Applied Physics Letter, 70(7), 1997, pp. 826-828
3. G. Bruno, P. Capezzuto and A. Madan, Plasma Deposition of Amorphous Silicon – Based Materials, Academic Press, Boston, 1995
4. A. L. Fahrenbruch and R. H. Bude, Fundamentals of solar cells, Academic Press, New York, 1983
5. M. Stutzmann, "Structural, optical, and spin properties of hydrogenated amorphous silicon-germanium alloys", Journal of Applied Physics, 66(2), 1989, pp. 569-592.
6. C. Graeff and I. Chambouleyron, "Structural and optoelectronic properties of Ge-rich hydrogenated amorphous silicon-germanium alloys", Journal of Applied Physics, 76(4), 1994, pp. 2473-2475
7. Mahan, L. Malhotra and S. Kashyap, "Electrical and optical properties of hydrogenated amorphous silicon germanium (a- $Si_{1-x}Ge_x$:H) films prepared by reactive ion beam sputtering", Journal of Applied Physics, 66(6), 1989, pp. 2528-2537

8. Y. Chou, S. Lee, "Structural, optical, and electrical properties of hydrogenated amorphous silicon germanium alloys", Journal of Applied Physics, v83, n8, 1998, pp. 4111-4123

9. V. L. Kuznetsov, M. Zaman, L. Vosteen B. Girwar and J. W. Metselaar, "Electrical and optical properties of plasma-deposited a-SiGe H alloys: Role of growth temperature and postgrowth anneal", Journal of Applied Physics, v80, n11, 1996, pp. 6496-6503

10. C. Graeff and M. Stutzmann, " Electrical detected magnetic resonance in a-Si:H/ a - Ge:H multilayers", Journal of Applied Physics, v79, n12, 1996, pp. 9166-9171

11. N. Saito, T. Yamaguchi and I. Nakaaki, " comparative study of properties between a-GeC:H and a-SiC:H films prepared by radio-frequency reactive sputtering in methane", Journal of Applied Physics, v78, n6, 1995, pp. 3949-3954

12. J.Yang, A.Banerjee, S.Guha, "Triple-junction amorphous silicon alloy solar cell with 14.6% initial and 13.0% stable conversion efficiencies", Appl. Phys. Lett., v70, n22, 1997, pp. 2975-2977

13. S. K. O'Leary, "Optical absorption, disorder, and the disorderless limit in amorphous semiconductors", Applied physics letter, v72, n11, 1998, pp. 1332-1334

14. S. Aljishi, J. Cohen S. Jin and L. Ley, " Band tails and thermal disorder in doped and undoped hydrogenated amorphous silicon and silicon –germanium alloys", Materials Research Society Symposium proceedings, v192, pp. 27-37, 1990

15. T. J. Mcmahon, "Defect equilibration in device quality α-Si:H and its relation to light-induced defects", Proc.Amer.Inst. of Phys., v234, 1991, pp. 83-90

16. A. Middya, A. Ray, S. Jones and D. Williamson, "Improvement of microstructure of amorphous silicon-germanium alloys by hydrogenated dilution", Journal of Applied Physics, 78, 1995, pp. 4966-4974

17. J. Lai, C. Liu , L. Chen and J. Cheng, " Formation of amorphous interlayer by solid-state diffusion in TI thin films on epitaxial Si-Ge layers on silicon and germanium", Journal of Applied Physics, 78(11), 1995, pp. 6539-6542

18. P. Donvan and P. Mangin, " Interpretation of transmission electron microscope images of amorphous silicon/germanium and silicon /iron multilayers", Journal of Applied Physics, 69(3), 1991, pp.1371-1376

19. I. Kato, T. Yoneda, T. Matsushita, "Influence of ion bombardment on α-Si:H films fabricated by plasma chemical vapor deposition", Electronics & Communications in Japan, Part II: Electronics (English translation of Denshi Tsushin Gakkai Ronbunshi), v78, n2, Feb 1995 pp. 70-78

20. K. Kato and I. Kato, "Deposition of hydrogenated amorphous silicon films using a microwave plasma chemical vapor deposition method with DC bias", Japanese Journal of Applied Physics, Part 1: Regular Papers & Short Notes, v30, n6, Jun 1991 pp. 1245-1247

21. X. Xu, J. Yang, S. Guha, "Effect of ion bombardment during deposition of amorphous silicon and silicon-germanium alloy solar cell", Journal of Non-Crystalline Solids Proceedings of the 1995 16th International Conference on Amorphous Semiconductors - Science and Technology. Part 2, Sep 4-8 1995, v198-200, npt2, May 2, 1996, Kobe, Jpn, pp. 1113-1116

22. S. Guha, X. Xu, J. Jiang and A. Banerjee, "Microwave glow discharge deposition of amorphous silicon based alloys at high deposition rates for solar cell application", Mat. Res. Soc. Symp. Proc., 377,1995, pp. 621-626

23. P. Wickboldt, D. Pang, W. Paul, "Improved α-$Si_{1-x}Ge_x$:H of large x deposited by PECVD", Journal of Non-crystalline Solids, 198-200, 1996 pp. 567-571

24. T. Sasaki, Y. Ichikawa, "Effect of ion bombardment during plasma CVD on the film properties of α-Si:H studied by IEC plasma CVD", Journal of Non-Crystalline Solids Proceedings of the 1995 16th International Conference on Amorphous Semiconductors - Science and Technology. Part 2 (of 2) Sep 4-8, 1995, v198-200, npt2 May 2, 1996 Kobe, Jpn, pp. 1007-1011

25. J. Dutta, K. Hasezaki, A. Mashima, "Effect of ion bombardment on the properties of hydrogenated amorphous silicon prepared from undiluted and Xenon-diluted silane", Japanese Journal of Applied Physics, Part 2: Letters, v31, n3B, Mar 15 1992 pp. L299-L302

26. S. Sugiyama, X. Xu, J. Jiang and S. Guha, "Light-induced degradation of amorphous silicon-germanium alloy solar cells deposited at high rates", Mat. Res. Soc. Symp. Proc., 420,1996, pp. 197-202

27. S. Haroon, Effect of Deposition Condition on Properties of a-(Si,Ge):H Films and Devices Using ECR-plasma Deposition, MS thesis, Iowa State University, 1998

28. S. Kaushal, Stability and Electronic Properties of Amorphous Silicon p-I-n Devices Fabricated Using ECR Plasma Enhanced Chemical Deposition, Ph.D. thesis, Iowa State University,1997

29. K. Mackenzie, P. LeComber and W. Spear, "The density of states in amorphous silicon determined by space-charge-limited current measurement", Philosophical Magazine B, 46, 1982, pp. 377-380

30. J. David Cohen, "Density of states from junction measurements in hydrogenated amorphous silicon", 21(C), Semiconductors and semimetals, 1984

31. W. denBoer, "Determination of midgap density of states in a-Si:H using space-charge-limited current measurements", Journal de Physique, 42,1981, pp. 451-454

32. D. Shen, J. P. Conde, V. Chu S. Wanger, " Carrier lifetime in amorphous semiconductors", Journal of Applied Physics,75(11), 1994, pp. 7349-7355

33. C. Palsule, U. Paschen and S. Guha, "Evidence for hole traps at the amorphous silicon/amorphous silicon-germanium heterostructure interface", Applied physics letter, 70(4), 1997, pp. 499-501

34. G. Baldwin, Design and modeling of a graded bandgap amorphous silicon solar cell deposited by plasma enhanced chemical vapor deposition, Ph.D. thesis, Iowa State University, 1994

35. V. Dalal, G. Baldwin and K. Han, " Deposition of High quality a-(Si, Ge):H films and novel grades gap devices using triode glow discharge deposition", Proceedings of 23rd IEEE PVSC, pp. 1037-1047, 1993

36. V. L. Dalal, S. Haroon, Z. Zhou, T. Maxson and K. Han , "Influence of plasma chemistry on the properties of a-(Si,Ge):H alloys", Journal of Non-Crystalline Solids, 266-269 (1-3) ,2000, pp. 675-679

37. V. L. Dalal, T. Maxson, S. Haroon, "Influence of plasma chemistry on the properties of amorphous (Si,Ge) alloy devices", Materials research society symposium – proceedings amorphous and microcrystalline silicon technology-1998 Proceedings of the 1998 MRS spring meeting, Apr 14-17 1998, v507, 1999, San Francisco, CA, pp. 441-446

38. V. L. Dalal, T. Maxson, K. Han, "Properties of a-Si:H and a-(Si,Ge):H solar cells prepared using ECR deposition techniques",; Conference record of the IEEE photovoltaic specialists conference proceedings of the 1997 IEEE 26th photovoltaic specialists conference, Sep 29-Oct 3 1997, Anaheim, CA, pp. 695-698

39. V. L. Dalal, R. Knox, B. Moradi, "Measurement of Urbach edge and midgap states in amorphous silicon p-i-n devices", Solar energy materials and solar cells, 31 (3), 1993, pp. 349-356

40. G. Baldwin, V. Dalal, K. Han, "Deposition of high quality a-(Si,Ge) :H films and novel graded gap devices using rf triode glow discharge deposition", Conference record of the IEEE photovoltaic specialist conference proceedings of the 23rd IEEE photovoltaic specialist conference, May 10-14 1993, Louisville, KY, pp. 1037-1042

41. V. L. Dalal, K. Han, "Research on a-(Si, Ge):H materials and devices", NREL subcontract XAK-8-17619-30, 1999.

42. Matthew DeFreese, Parameter measurements of a germane Electron Cyclotron Resonance plasma, MS thesis, Iowa State University, 2000

ACKNOWLEDGEMENTS

I would like to take this opportunity to express my sincere gratitude to my major professor, Dr. Dalal for his invaluable guidance and encouragement throughout my research. Without his help, I can not finish my Ph.D. program successfully. Also I would like to thank Dr. Tuttle, Dr. Black and Dr.Shinar and Dr. Lynch for serving as my committee member and giving me some suggestions on writing my dissertation.

I would like to thank Kay Han and Tim Maxon for their helping in sample preparation. Also thank Caustoosh Bezbaush and Yong Liu and other students in MRC for their help and friendship.

I would like to take this chance to express my deepest affection to my parents for their support, patience and love throughout these years.